12-2021

Investigating Effects of Microenvironmental Stress on Cell Metabolism using Multiphoton Imaging

Lisa Rebello
University of Arkansas, Fayetteville

Investigating effects of microenvironmental stress on cell metabolism using multiphoton imaging

This dissertation submitted in partial fulfillment
of the requirements for the degree of
Doctor of Philosophy in Cell and Molecular Biology

by

Lisa Rebello
University of Pune
Bachelor's in Pharmacy, 2010
Uppsala Universitet
Master's in Biomedical Sciences, 2013

December 2021
University of Arkansas

This dissertation is approved for recommendation to the Graduate Council

_____
Narasimhan Rajaram, Ph.D.
Dissertation Director

_____
Timothy J. Muldoon, M.D., Ph.D.
Committee Member

_____
Robert J. Griffin, Ph.D.
Committee Member

_____
Tameka A. Bailey, Ph.D.
Committee Member

_____
Leonard A. Harris, Ph.D.
Committee Member

ABSTRACT

Resistance to therapy in cancer is a major cause of poor prognosis in patients. Tumor hypoxia plays an active role in mediating treatment resistance and has been linked to metastases and metastatic potential in cancer. Our research focused on three objectives: i) To understand metabolic effects of chronic and intermittent hypoxia in murine breast cancer cells and its affiliation with metastatic potential ii) To identify the metabolic changes associated with radiation therapy in a panel of radiosensitive and radioresistant human head and neck cancer cells and iii) to monitor the changes in cell metabolism associated with gain of treatment resistance. To detect these changes, we employed optical imaging of endogenous fluorophores with two-photon excited fluorescence (TPEF) to quantify cellular metabolism. Our studies with cancer cells exposed to hypoxic stress revealed that chronic hypoxia led to changes in cellular metabolism in only poorly metastatic cancer cells while intermittent hypoxia exposure had no effect on cellular metabolism in any cancer cells. While hypoxia is known to lead to stable expression of the transcription factor – hypoxia-inducible factor (HIF-1), there are other microenvironmental stresses, such as radiation therapy that can cause activation of HIF-1. Therefore, we next investigated changes in cellular metabolism in a panel of head and neck cancer cells using TPEF and determined if the radiation-induced changes in metabolism were driven by HIF-1. Our final study involved investigating the effects of radiation therapy on cellular metabolism in a panel of isogenic cell lines that had increasing levels of radiation resistance. We found that wild type cells exhibit transformations in cellular metabolism on exposure to varied treatments while moderately resistant cells show changes in cell metabolism on exposure to HIF-1 inhibitor, YC-1 and combination of YC-1 and radiation. Conversely, there were no changes in radiation-r-resistant cells on exposure to any therapy. This present study demonstrates the ability of optical metabolic imaging to provide new insights into understanding treatment resistance in cancer cells.

DEDICATIONS

“I didn’t succumb to stereotype that science wasn’t for girls.”

-Sally Ride

This dissertation is dedicated to all the women in science, known and unknown, who have made a mark and those trying to shatter the glass ceiling of patriarchy to make a mark.

May our tribe increase!

ACKNOWLEDGEMENTS

I would like to pay respect and deepest gratitude to Dr. Narasimhan Rajaram, my advisor, for his guidance throughout this journey. He not only believed in me but also encouraged me to believe in myself whenever I lacked confidence in my ability as a researcher.

I am grateful to Dr. Dings and Samir for providing the resistant cancer cell lines which formed the basis of my third manuscript. I am also thankful to Dr. Muldoon for patiently answering my queries and guidance towards using the two-photon microscope.

I am thankful to Dr. Bailey for important and meaningful discussions relating to research, gender, and racial representations in science.

I am highly appreciative of Mr. Jared McPeake who worked with me on this project. I am also thankful to Mr. Davin Means for helping with cell culture work around the lab.

I am grateful to my lab mates Joel and April for their excellent collaborations and friendships.

Miren Tanna, Samruddhi and Dobby: Big shoutout for being there for me during my initial days in NWA. I am truly grateful for all the help and for getting acquainted with the new place.

Swati Ravi, thank you for being there for me to listen to my complaints and crazy conversations.

BanuPriya Sridharan, for being a patient mentor throughout my internship and helping me appreciate automation in the industrial setting.

I am indebted to my friends: Olivia Kolenc, Rudy Acosta, Ishita Tandon, Oliver Baptista, Christine Shamblin and Haley James for cherished friendships and good times.

Finally, I would like to thank my mom, Senora and Uncle Malcolm without whom this journey would have been impossible. Their never-ending love and patience helped me a lot during this journey. I wish my grandmother; Mrs. Rosemary Falcao would be alive to see me graduate with this doctoral degree. Last but not the least, I would like to thank Rosario Cervellere for being a rock support in this scientific journey.

LIST OF CONTENTS

Chapter 1:

Introduction

Cancer Statistics and factors influencing cancer:

The word “cancer” has its origins in the Greek word “karkinos[1]”. Cancer is characterized by uncontrolled cell growth ultimately leading to metastasis that is invasion of cancer cells to neighboring organs other than the primary site[2]. Risk factors for cancer include age, family history, tobacco, alcohol, obesity, viral infections such as human papillomavirus (HPV), exposure to radiation and certain carcinogenic chemicals[3]. According to Global Cancer Observatory (GLOBOCAN), 1,806,590 newer cases of cancer and 10 million deaths from cancer were predicted in the year 2020[4]. Surgery followed by radiation and/or chemotherapy is a treatment of choice in most cancers[5]. Treatment resistance in patients is a major cause of metastases, that is, infiltration of cancer cells to secondary sites resulting in mortality[6]. Treatment resistance in cancer cells arises due to inherent mutations or modifications in tumor microenvironment[7] (TME). One of the critical factors that drive these changes in tumor cells is tumor hypoxia. Tumor hypoxia plays a critical role in cancer progression and determining patient outcome[8].

Tumor Hypoxia

One of the hallmarks of cancer listed by Weinberg et al is judicious growth and proliferation of tumor cells[9]. To sustain this growth of tumor, it must be equipped with vasculature that provides the cells with oxygenation and nutrients. Increased proliferation in tumor cells leads to absence of vasculature or underdeveloped vasculature leading to oxygen deficiency. Tumor hypoxia is generated as a consequence of imbalance between cellular oxygen consumption rate and supply of oxygen to the cells[10]. Some of the prominent factors by which hypoxia is generated in

the tumor microenvironment are as follows: perfusion-related, diffusion related anemic hypoxia. Perfusion related hypoxia is generated because of faulty vasculature leading to inadequate blood flow. Tumor growth and proliferation leads to an increase in diffusion distances ensuing diffusion related hypoxia. This is mostly observed in cells that are at a distance >70μm. Anemic hypoxia is induced in tumors due to decreased oxygen transport capacity resulting in tumor associated or therapy induced anemia[11]. Hypoxia is a feature observed in most tumors and is associated with poor prognosis[12,13,14,15]. This is because tumor hypoxia grants resistance to cancer cells towards therapeutic agents firstly by restricting the amount of oxygen that is pivotal for the cytotoxic effect of the therapeutic agents but also by promoting cell cycle arrests, suppressing apoptosis, influencing drug delivery as well as cellular uptake of the chemotherapeutic agents[16,17,18]. In case of radiation therapy, oxygenation plays a significant role as well oxygenated cells are susceptible to radiation while hypoxic cells are resistant to it as oxygen reacts with free radicals in DNA generated by ionizing radiation driving permanent damage[17,19]. Furthermore, it has been proven that cells that are resistant to therapy are passive, less proliferating with stem cell-like properties resides in the hypoxic regions of the tumors[20,21]. Therefore, hypoxia promotes stem cell like phenotype, reduces senescence, disorganized angiogenesis, metastases and treatment resistance[22,23,24,25,26,27,28]. This cellular remodeling by hypoxia is intervened by a transcriptional regulator, Hypoxia Inducible Factor-1 (HIF-1). HIF family comprises of HIF-1, HIF-2, and HIF-3 with α and β subunits that disintegrate in normoxic conditions[29]. Overexpression of HIF-1 is generally observed in tumor cells while certain subgroups of tumor- associated macrophages highly express HIF-2. HIF-3 is expressed in pulmonary alveolar epithelial cells and human kidney[30]. Activation of HIF-1 subunits and their stabilization (HIF-1α, HIF-2α, HIF-3α) is determined by Prolyl Hydroxylase (PHD) and Factor Inhibiting HIF-1 (FIH-1)[31]. Although HIF-1α is expressed universally in all cell types[32], HIF-2α is expressed only in distinct cell types[33]. Intratumoral hypoxia and genetic alterations like gain- of-function or loss-of- function mutations in genes lead to higher expression of HIF-1α in many

human cancers[34]. HIF-1α is rapidly destroyed in normoxic conditions through ubiquitin-mediated process which is activated by pVHL (von-Hippel- Lindau protein) a tumor suppressor protein. Lower oxygen levels lead to stabilization of HIF-1α leading to its translocation in nucleus wherein it binds to HIF-1β ultimately culminating into HIF-1 activation[35].

Although hypoxia activates HIF-1, it can be generated in response to other alternative stress factors. Free radicals are produced on exposure to ionizing radiation in DNA. Peroxy radical (DNA-OO˙) is produced when free radicals in DNA (DNA˙) react with the available oxygen leading to chemical modifications in the DNA ultimately causing cell death. In case of oxygen deficiency, reduction of DNA radical takes place causing restoration of DNA to its original composition (DNA H) eventually influencing cell survival[36]. Treatment outcome employing fractioned therapy in patients is highly improved by reoxygenation causing radiosensitization of hypoxic cancer cells[37]. Nonetheless, an unintended consequence of tumor reoxygenation post radiation is buildup of ROS, that further leads to stabilization of HIF-1 even under well-oxygenated conditions[38,39]. HIF-1 instantaneously targets several genes that are linked to glycolysis leading to glucose catabolism under oxygenated conditions[40,41,42,43,44]. This change to higher glucose catabolism can stimulate radiation resistance via pentose phosphate shunt to maintain the NADPH- glutathione buffer thereby scavenging radiation- induced ROS[45]. Furthermore, it also generates higher lactate production, which is an important ROS scavenger, causing reduced radiosensitivity[46].

HIF-1 also determines the direct and indirect regulation of more than 100 genes like vascular endothelial growth factor (VEGF), glucose transporter 1, glucose transporter 3, insulin-like growth factor binding protein-1 and -3, insulin-like growth factor II, transforming growth factor-β3 and p21 which advances angiogenesis, cell growth and proliferation, invasion/metastasis, and metabolic reprogramming[47]. Activation of phosphatidylinositol 3-kinase (PI3K) and ERK

mitogen-activated protein kinase (MAPK) pathways by tyrosine kinase receptors, non- receptor tyrosine kinases or G-protein-coupled receptors induces the protein synthesis of HIF-1α[29]. One of the important enzymes upregulated due to tumor hypoxia is carbonic anhydrase IX(CAIX)[48]. In normal cellular functioning, CAIX catalyzes the hydration of carbon dioxide to bicarbonate ions and protons and is an important reaction regulating acid-base balance in subcellular components in the plasma membrane[49]. In tumor cells, induction of CAIX by hypoxia leads to generation of acidic by products sustaining the tumor cell proliferation. Additionally, it supports angiogenesis, epithelial- mesenchymal transition, invasiveness, enhancing tumor-stroma crosstalk[48]. A recent study has pointed out that colon cancer cells that express hypoxia receptor carbonic anhydrase IX (CA IX) on treatment with CA IX inhibitors results into decreased growth in the tumor cells[50].

In 1955, Gray et al laid the groundwork identifying the relationship between tumor hypoxia with radioresistance in cancer cells[51]. Lately, studies have pointed that HIF-1 plays a critical role in inducing treatment resistance in cancer[52,53]. Many studies have demonstrated that HIF-1α is expressed in radioresistant cells at normal oxygen levels. Additionally, post radiation has led to a considerable increase in the HIF-1α expression as compared to pre-radiation in radiation resistant cells[54]. Another study conducted by Milosevic et al in 247 patients with prostate cancer demonstrated relapse post radiotherapy with local recurrence in tumors exhibiting hypoxia[55,53]. A study conducted by Dales et al in 745 patients with breast cancer exhibited increased metastatic risk with higher expression of HIF-1, transcription factor for hypoxia with decrease in survival rate[56].

However, tumors experience large spatial and temporal variations in hypoxia that lead to different outcomes[57]. The heterogenic hypoxic exposure in tumors arises from the following factors: 1) chronic hypoxia resulting from restricted diffusion of oxygen from blood vessels to the

tumor cells owing to distance (>70 µm) 2) varied red blood cell (RBC) flux and large blood viscosity 3) proliferating tumor cells causing narrowing of blood vessels[58,59]. Martinive et al found out that intermittent hypoxia in conjunction with radiation therapy led to 50% decrease in cell death and faster cell growth[60]. Another study determined that intermittent hypoxia leads to downregulation of ER- alpha expression leading to reduced therapeutic response in tumors and development of resistance towards therapy[61]. In studies involving animal models, intermittent hypoxia increased the chances of lung metastases in mice with xenografts[62]. Additionally, tumor hypoxia and expression of its transcription factor HIF-1 plays a crucial function in elucidating survival rate in head and neck cancer patients[63]. Recently, a study by Alhallak et al has found that isogenic radiation resistant cells inherently expressed higher HIF-1α as compared to its radiosensitive counterpart at normoxic conditions[54]. Furthermore, Lee et al investigated long term changes in tumor cell metabolism on exposure to radiation and combination therapy and found that blocking the HIF-1α pathway not only leads to an increase in redox ratio as an output of cellular metabolism, but also lead to an increase in ROS production, mitochondrial clustering, and glucose uptake[64].

Tumor cell metabolism:

Cellular metabolism is one of the key features of the tumor microenvironment[65]. Cellular metabolism can be described as chemical reactions that transform nutrients into energy and building blocks of body that sustain growth and development [66]. One of the key molecules that drive energy dependent cellular mechanisms is Adenosine triphosphate (ATP) and is essentially produced by two key metabolic pathways: glycolysis and oxidative phosphorylation (OXPHOS). Glycolysis, wherein glucose is converted to pyruvate in cytoplasm, generates 2 molecules of ATP while OXPHOS leads to routing of pyruvate to the tricarboxylic acid (TCA), or Krebs, cycle in the mitochondria, generates 30 molecules of ATP per molecule of glucose. Lower oxygen levels lead to anaerobic glycolysis modifying pyruvate into lactate which is a very inefficient way

of producing energy[67]. In presence of adequate oxygen levels, a more efficient process OXPHOS occurs in mitochondria. Compared to normal cells, cancer cells undergo to aerobic glycolysis also known as “Warburg effect [68].” To maintain this high rate of glycolysis, cancer cells switch from aerobic glycolysis to uncouple ATP generation from electron transport chain in the mitochondria. As a result, tumor cells can expend nicotinamide adenine dinucleotide (NADH) a key metabolic coenzyme without production of ATP thereby transforming the intermediate glycolytic products into non-ATP producing bypass mechanisms[67]. Modifications in the metabolic pathways consequently lead to changes in the mitochondria and other cellular organelles[69]. Variation in the functioning of the oncogenes like Ras or Myc results in the activation of transcription factors like HIF-1 initiating influx of glucose and suppression of OXPHOS. Consequently, this prompts the activation of pentose phosphate pathway(PPP) or amino acid biosynthetic pathways[70].

Increased reactive oxygen species (ROS) production leading to enhanced cell proliferation is another key characteristic of tumor cell metabolism[70].To combat apoptosis driven by larger volumes of ROS, the tumor cells produce larger volumes of NADPH in the cytosol and mitochondria. Additionally, mitochondrial ROS is responsible for buildup of oncogenic DNA abnormalities triggering oncogenic signaling pathways[71]. Furthermore, activation of ROS scavenging system leads to an increase in lipid biosynthesis to protect and sustain the growth of tumor[72].

Fatty acids support the functioning of signaling molecules, membrane assembly molecules and bioenergetic substrates. Several studies have demonstrated the lower expression of adipose triglyceride lipase (ATGL) an enzyme that engenders the catalysis of triacylglycerols in many cancer subtypes. In the context of tumor cell metabolism, ATGL is associated with proliferator-activated receptor-α (PPAR-α) signaling and other metabolic pathways related to inflammation, autophagy, and redox homeostasis. These pathways are critical in inducing the growth of tumor and ultimately metastases[70]. Downregulation of ATGL has resulted in the metabolic switch from

OXPHOS to glycolysis which is one of the hallmarks of cancer mentioned by Weinberg[73]. Dysregulation in the lipid function also results in morphological change in the mitochondria which ultimately causes a reduction in OXPHOS expression and need for substitute source of energy[74].

In summary, we have literature backing the fact that tumor hypoxia plays a critical role in tumor cell metabolism that contributes towards treatment resistance followed by metastases ultimately leading to poor prognosis. However, there remains a gap in knowledge about the changes in cellular metabolism in cancer cells that drive the treatment resistance and metastasis fueled by hypoxia.

Multiphoton Imaging: Optical Redox Ratio (ORR)

One of the promising pre-clinical techniques to evaluate cell metabolism is via optical imaging of endogenous fluorescent metabolic cofactors, nicotinamide adenine dinucleotide (NADH) and flavin adenine dinucleotide (FAD)[75]. Optical imaging of these endogenous fluorophores or biomarkers was first conceptualized and reported by Britton Chance in 1950's while establishing the connection between redox state of respiratory enzymes and spectra, reaction kinetics in whole as well as homogenized cells[76]. Furthermore, Chance et al demonstrated the interconnection between changes in intracellular redox states of pyridine nucleotides because of fluorescence produced due to reduced pyridine nucleotides in mitochondria in rat brain cortex and kidney employing microfluorometry[77,78]. Additionally, a recent study by Xu et al reported a novel redox imaging method to quantitatively determine the concentration of NADH and flavoproteins (Fp) exhibiting the intracellular mitochondrial redox state in an *in vivo* set up using a low temperature 3D optical redox scanner which was previously developed by Britton Chance[79].

The idea of two-photon scanning fluorescence microscopy was first developed and later patented by Winfried Denk, James Strickler and Watt W. Webb in 1990 although the theoretical

concept of two-photon absorption by atoms was the innovative brainchild of Maria Goeppert Mayer[80,81]. The source of two-photon excitation results from synchronous absorption of two photons in a single event. To understand two photon excitation, we should consider one-photon excitation or single photon excitation. In a one-photon excitation, a fluorophore exists in ground state S_0 and elevates into an excited state S_1 after the absorption of a photon. After a moment in the excited state, the fluorophore bounces back to its original state subsequently emitting a photon. For successful excitation of fluorophore, every fluorophore should have a wavelength (λ) and energy (E) that equals the energy of the excited state of fluorophore. For proficient excitation of fluorophore from ground state to excited state, the energy required is given by the formula:

$$\boldsymbol{Es1 - Es0 = hc/\lambda}$$

where $Es1$ is the energy of the fluorophore in the excited state, $Es0$ is the energy of the fluorophore in the ground state, h is Planck's constant= 6.626176 x 10^{-34} joule-seconds, c is the speed of light 3x10^8 m/s.

In case of two photon excitation wherein there is simultaneous absorption of two photons in a single event, each photon possesses half the energy as compared to a single-photon absorption. The photons in a two-photon excitation must acquire wavelength nearly twice that in case of photons in a one-photon excitation in a similar situation as the energy of a photon is inversely proportional to its wavelength. Therefore, the ensuing fluorescent intensity in a two-photon excitation relies upon the square of excitation intensity, which is supported by an ultra-short, pulsed laser source and a two-photon excitation microscopy.

An ultra-short, pulsed laser source ensures that the two photons in a two-photon excitation are absorbed simultaneously in approximately 10^{-18} seconds affirming the possibilities of occurrence of two photons at the fluorophore at the same time. Additionally, a high numerical aperture (NA) objective generates convergence of photons thereby expanding the likelihood of two photons coincident at the fluorophore concurrently. All these factors contribute towards

higher focus at the center in a two-photon excitation microscopy leading to one of its advantage over one-photon excitation. Another advantage is the decrease in the chances of photobleaching and phototoxicity that can occur in live cells and tissues. Moreover, as compared to a conventional confocal microscope, imaging depth with a two-photon excitation is greater and falls in the range of 200µm to 1mm which is contingent upon the type of tissue, intensity of labelling at the target and the caliber of the laser[81,82]. Overall, two photon microscopy is a non-invasive, label free technique with a deeper light penetration as compared to classic microscopic techniques.

NADH and FAD stimulate the generation of fluorescence that can be exploited to determine metabolic activity of different organs under different physiological conditions. Majority of the fluorescence from NADH and FAD originates from mitochondria wherein oxygen is employed to produce Adenosine Triphosphate (ATP). The ratio of FAD/ (FAD + NADH), known as the optical redox ratio (ORR) can be potentially used for evaluation of cell metabolism[83] and to investigate changes in cell metabolism in cell differentiation and malignant transformation[84,85]. Furthermore, evidence suggests high optical sensitivity that could be used to evaluate vital changes in cell metabolism that are characteristic of metastatic ability and invasiveness of the cancer cells[86]. Recent investigation by Alhallak et al. has demonstrated that ORR could be used as an instantaneous approach for early detection of radiation resistance based on early shifts in metabolism of cancer cells[64]. Another investigation by Pouli et al determined metabolic changes in live human cervical biopsies that are indicative of diagnosing precancerous growths[87].

Application of metabolic imaging in-response to therapy:

The choice of therapy for cancer depends on various factors; predominantly the location of the primary tumor, type of cancer and histopathological classification of tumor play an important role[88]. Treatment choices for cancer vary from having only one type of treatment or a combination of treatments like surgery followed by chemotherapy and / or radiotherapy,

immunotherapy, hormone therapy etc[89]. One of safest, non-invasive approaches to monitor molecular processes in is metabolic imaging in-response to therapy. Radionuclide imaging has facilitated contrast imaging in studies related to cancer cell metabolism and receptor expression. This technique is highly specific and receptive to cell death and therefore used to detect metabolic shifts in tumor cells in response to therapy by administering low doses of the radionuclides. One of the key advantages of this method is that it doesn't exhibit any adverse pharmacological effects from the radionuclides. Secondly, many recent studies have demonstrated that small tracer molecules have been employed for quick tumor penetration and clearance. The disadvantages of this technique are the detection of emission signal and the number of times a patient would be injected with radionuclides and imaged while undergoing therapy[90].

Magnetic Resonance Imaging (MRI) methods are responsive towards identifying changes in the cellular level that are associated with cell death processes, like apoptosis, macromolecular changes, influx of water and water exchange across the cellular membrane etc. The major drawback with techniques that utilize MRI is the low signal to noise ratio[90].

Dynamic contrast-enhanced ultrasound (DCE-US) shares some of the benefits of the ultrasound techniques such as- fast, portable, safe, widely available and cost effective. It enhances the properties of microbubble contrast agents in tracking the therapeutics that target blood perfusion. Constraints due to regulatory hurdles has limited the utilization of microbubble agents in their clinical approval in many countries[91].

One of the non-invasive imaging techniques that has been demonstrated to be useful to monitor treatment response in breast cancer patient is diffuse optical imaging[92]. The limitation of this technique is its application restricted to tissues like breast and brain due to depletion of near-infrared light in soft tissues[93].

Fluorodeoxyglucose-positron emission tomography (FDG-PET) is a frequently used technique in the clinic to detect glycolytic metabolism in tumors and track their response to treatment[94].

Metabolic reprogramming in tumors is a key emerging hallmark of cancer. New research has highlighted that metabolic reprogramming involves a highly complex pathways that eventually facilitates the cells to boost the employment of a various set of substrates and nutrients to expand and adapt their microenvironment to bypass death and ultimately metastasize[95]. Therefore, there is an unmet need for imaging modalities with higher sensitivities to metabolic changes with superior resolution and *in vivo* applications. Some of the key gaps that can be addressed, particularly in context of non-destructive, increased imaging depth, reduced phototoxicity and multi-parametric metabolic functional imaging is by employing optical, non-linear microscopic imaging methods.

Monitoring treatment response with optical metabolic imaging:

In the past couple of years, optical imaging employing multiphoton microscopy has been implemented in various diseases for deeper understanding into elucidating the metabolic changes in the cells and modifications to the extracellular matrix (ECM) in normal cells versus the diseased counterparts[96]. Two-photon excitation microscopy not only elucidates deep tissue imaging (up to 1000µm) but also allows for three-dimensional imaging as compared to confocal microscopy[82]. This technique allows for out of background light rejection because of its spatial confinement leading to higher concentration of photons at the focal point[87]. Owing to its ability to reduce phototoxicity, it has promoted long term imaging of photosensitive biological samples. On the contrary, high intensity two photon illumination has been used to generate ROS in minuscule amounts in cardiomyocytes further studying its effects on cell metabolism[97]. Unlike Sea Horse Metabolic analysis, two-photon microscopy has the capability to potentially detect cellular heterogeneity in a sample which would be beneficial in identifying cells with higher metastatic phenotype in tumors.

The Chance Redox Scanner was first conceptualized by Britton Chance as mentioned earlier has been used extensively to study cancer. Studies have demonstrated its capability in

differentiating between normal and cancerous breast tissue biopsies from patients Recently, studies have shown that optical imaging was able to identify between estrogen receptor positive (ER+) breast tumors, estrogen negative (ER-) tumors and normal breast tissues because redox ratio in ER- and ER+ tumors is relatively lower than the normal breast tissues[98]. Additionally, studies have depicted that optical imaging could detect the glycolytic status, sub-types and predicting treatment responses and metastatic potential in a panel of breast cancer cells[99,100,101]. The application of optical imaging isn't limited to only one cancer subtype. Furthermore, a study has highlighted that optical imaging was able to elucidate the treatment response in head and neck cancer cells[102]. Optical imaging in head and neck cancer organoids could identify various heterogenous tumor cell populations and has opened channels for a potential setting in a high-throughput assay in the drug discovery process[103]. Microfluidic model that simulates the mammary duct in the ductal in situ carcinoma (DCIS) in which a co-culture of various cell types was seeded was first developed by Bischel et al[104]. This model was later adapted by Ayuso et al to study the growth and metabolism of cells involved in DCIS. Optical imaging could identify the generation of various metabolic signatures within the lumen across hypoxic and nutrient gradients thereby providing insights into changes in metabolism from DCIS to an invasive ductal carcinoma[105]. Recently a study by Gil et al has demonstrated that optical imaging could track prolonged changes in the structure as well as metabolism arising from treatments in patient derived cancer organoids[106]. Apart from studying tumor cell metabolism, optical imaging has could identify changes in the cellular metabolism associated with stem cell differentiation[85], assimilation of donor cells post intracardiac transplantation with respect to its functionality[107], calcium signaling in cardiomyocytes[108] etc.

With the evolution of chromophores with increased two photon excitation, future developments in the optical imaging using two photon microscopy would lead to an increase with higher imaging depths Improvement in the laser bandwidth might enhance imaging depth thereby

reducing photobleaching and photodamage. Finally, combining two-photon microscopy with other techniques would support new scopes for discovering new aspects of cell metabolism[109].

References:

1. Papavramidou, N., Papavramidis, T. & Demetriou, T. Ancient greek and greco-Roman methods in modern surgical treatment of cancer. *Ann. Surg. Oncol.* **17**, 665–667 (2010).

2. NIH. What Is Cancer ? Differences between Cancer Cells and Normal Cells. *Natl. Cancer Inst.* 1–8 (2021).

3. Cancer.Net. Understanding Cancer Risk. *https//www.cancer.net/navigating-cancer-care/prevention-and-healthy-living/understanding-cancer-risk Cancer.Net Editor. Board, 03/2018. Erişim tarihi 19.11.2019* 10–12 (2018).

4. Sung, H. *et al.* Global Cancer Statistics 2020: GLOBOCAN Estimates of Incidence and Mortality Worldwide for 36 Cancers in 185 Countries. *CA. Cancer J. Clin.* **71**, 209–249 (2021).

5. Maramaldi, P., Dungan, S. & Poorvu, N. L. Cancer treatments. *J. Gerontol. Soc. Work* **50**, 45–77 (2008).

6. Mansoori, B., Mohammadi, A., Davudian, S., Shirjang, S. & Baradaran, B. The different mechanisms of cancer drug resistance: A brief review. *Adv. Pharm. Bull.* **7**, 339–348 (2017).

7. Housman, G. *et al.* Drug Resistance in Cancer: An Overview. *Cancers (Basel).* **6**, 1769–1792 (2014).

8. Jing, X. *et al.* Role of hypoxia in cancer therapy by regulating the tumor microenvironment. *Mol. Cancer* **18**, 1–15 (2019).

9. Hanahan, D. & Weinberg, R. A. Hallmarks of cancer: The next generation. *Cell* (2011). doi:10.1016/j.cell.2011.02.013

10. Brahimi-Horn, M. C., Chiche, J. & Pouysségur, J. Hypoxia and cancer. *Journal of Molecular Medicine* (2007). doi:10.1007/s00109-007-0281-3

11. Response, C. O ncologist. **9**, 4–9 (2004).

12. Brizel, D. M., Sibley, G. S., Prosnitz, L. R., Scher, R. L. & Dewhirst, M. W. Tumor hypoxia adversely affects the prognosis of carcinoma of the head and neck. *Int. J. Radiat. Oncol. Biol. Phys.* **38**, 285–289 (1997).

13. Rundqvist, H. & Johnson, R. S. Tumour oxygenation: Implications for breast cancer prognosis. *J. Intern. Med.* **274**, 105–112 (2013).

14. Schindl, M. *et al.* Overexpression of hypoxia-inducible factor 1α is associated with an unfavorable prognosis in lymph node-positive breast cancer. *Clin. Cancer Res.* **8**, 1831–1837 (2002).

15. Theodoropoulos, V. E. *et al.* Hypoxia-inducible factor 1α expression correlates with angiogenesis and unfavorable prognosis in bladder cancer. *Eur. Urol.* **46**, 200–208

(2004).

16. Vaupel, P. & Mayer, A. Hypoxia in cancer: Significance and impact on clinical outcome. *Cancer and Metastasis Reviews* (2007). doi:10.1007/s10555-007-9055-1

17. Pires, I. M. *et al.* Effects of acute versus chronic hypoxia on DNA damage responses and genomic instability. *Cancer Res* **70**, 925–935 (2010).

18. Bristow, R. G. & Hill, R. P. Hypoxia and metabolism: Hypoxia, DNA repair and genetic instability. *Nature Reviews Cancer* (2008). doi:10.1038/nrc2344

19. Bristow, R. G. & Hill, R. P. Hypoxia and metabolism: Hypoxia, DNA repair and genetic instability. *Nature Reviews Cancer* **8**, 180–192 (2008).

20. Carnero, A. & Lleonart, M. The hypoxic microenvironment : A determinant of cancer stem cell evolution. 96–105 (2016). doi:10.1002/icl3.1039

21. MICHA, R. 乳鼠心肌提取 HHS Public Access. *Physiol. Behav.* **176**, 100–106 (2017).

22. Muz, B. *et al.* The role of hypoxia in cancer progression, angiogenesis, metastasis, and resistance to therapy. doi:10.2147/HP.S93413

23. Chen, G. *et al.* Hypoxia induces an endometrial cancer stem-like cell phenotype via HIF-dependent demethylation of SOX2 mRNA. *Oncogenesis* **9**, (2020).

24. Chen, A. *et al.* Intermittent hypoxia induces a metastatic phenotype in breast cancer. *Oncogene* doi:10.1038/s41388-018-0259-3

25. Zhang, X., Li, J., Sejas, D. P. & Pang, Q. Hypoxia-reoxygenation induces premature senescence in FA bone marrow hematopoietic cells. *Blood* (2005). doi:10.1182/blood-2004-08-3033

26. Daly, C. S. *et al.* Hypoxia modulates the stem cell population and induces EMT in the MCF-10A breast epithelial cell line. *Oncol. Rep.* (2018). doi:10.3892/or.2017.6125

27. Olbryt, M. *et al.* Global gene expression profiling in three tumor cell lines subjected to experimental cycling and chronic hypoxia. *PLoS One* **9**, (2014).

28. Hsieh, C. H., Lee, C. H., Liang, J. A., Yu, C. Y. & Shyu, W. C. Cycling hypoxia increases U87 glioma cell radioresistance via ROS induced higher and long-term HIF-1 signal transduction activity. *Oncol. Rep.* (2010). doi:10.3892/or-00001027

29. Semenza, G. L. Targeting HIF-1 for cancer therapy. *Nature Reviews Cancer* **3**, 721–732 (2003).

30. Ke, Q. & Costa, M. Hypoxia-Inducible Factor-1 (HIF-1). **70**, 1469–1480 (2006).

31. Kaelin, W. G., Ratcliffe, P. J. & Semenza, G. L. Pathways for oxygen regulation and homeostasis: The 2016 albert lasker basic medical research award. *JAMA - J. Am. Med. Assoc.* **316**, 1252–1253 (2016).

32. Weidemann, A. & Johnson, R. S. Biology of HIF-1α. *Cell Death Differ.* **15**, 621–627 (2008).

33. Robinson, P. J., Hack, C. E., Foundation, H. M. J., Merrill, E. A. & Mattie, D. R. Mathematical modelling of the HIF-1 mediated hypoxic response in tumours. 49 (2017).

34. Zimna, A. & Kurpisz, M. Hypoxia-Inducible factor-1 in physiological and pathophysiological angiogenesis: Applications and therapies. *Biomed Res. Int.* **2015**, (2015).

35. Goda, N. & Kanai, M. Hypoxia-inducible factors and their roles in energy metabolism. *Int. J. Hematol.* **95**, 457–463 (2012).

36. Simon, M. C. Abstract SY34-02: The impact of O 2 availability on human cancer . **8**, SY34-02-SY34-02 (2010).

37. Fowler, J. F. The rationale of dose fractionation. in *The Relationship of Time and Dose in the Radiation Therapy of Cancer* 6–23 (Karger Publishers, 1969).

38. Moeller, B. J., Cao, Y., Li, C. Y. & Dewhirst, M. W. Radiation activates HIF-1 to regulate vascular radiosensitivity in tumors: Role of reoxygenation, free radicals, and stress granules. *Cancer Cell* (2004). doi:10.1016/S1535-6108(04)00115-1

39. Moeller, B. J. *et al.* Pleiotropic effects of HIF-1 blockade on tumor radiosensitivity. *Cancer Cell* **8**, 99–110 (2005).

40. Kim, J., Tchernyshyov, I., Semenza, G. L. & Dang, C. V. HIF-1-mediated expression of pyruvate dehydrogenase kinase: a metabolic switch required for cellular adaptation to hypoxia. *Cell Metab.* **3**, 177–185 (2006).

41. Papandreou, I., Cairns, R. A., Fontana, L., Lim, A. L. & Denko, N. C. HIF-1 mediates adaptation to hypoxia by actively downregulating mitochondrial oxygen consumption. *Cell Metab.* **3**, 187–197 (2006).

42. Luo, W. *et al.* Pyruvate kinase M2 is a PHD3-stimulated coactivator for hypoxia-inducible factor 1. *Cell* **145**, 732–744 (2011).

43. Sun, Q. *et al.* Mammalian target of rapamycin up-regulation of pyruvate kinase isoenzyme type M2 is critical for aerobic glycolysis and tumor growth. *Proc. Natl. Acad. Sci.* **108**, 4129–4134 (2011).

44. Zhong, J. *et al.* Radiation induces aerobic glycolysis through reactive oxygen species. *Radiother. Oncol.* **106**, 390–396 (2013).

45. Mims, J. *et al.* Energy metabolism in a matched model of radiation resistance for head and neck squamous cell cancer. *Radiat. Res.* **183**, 291–304 (2015).

46. Sattler, U. G. A. *et al.* Glycolytic metabolism and tumour response to fractionated irradiation. *Radiother. Oncol.* **94**, 102–109 (2010).

47. Masoud, G. N. & Li, W. HIF-1α pathway: Role, regulation and intervention for cancer

therapy. *Acta Pharm. Sin. B* **5**, 378–389 (2015).

48. Pastorekova, S. & Gillies, R. J. The role of carbonic anhydrase IX in cancer development: links to hypoxia, acidosis, and beyond. *Cancer Metastasis Rev.* **38**, 65–77 (2019).

49. Occhipinti, R. & Boron, W. F. Role of carbonic anhydrases and inhibitors in acid–base physiology: Insights from mathematical modeling. *Int. J. Mol. Sci.* **20**, (2019).

50. Pyrho, S. Expression of carbonic anhydrase IX suggests poor outcome in rectal cancer Clinical Studies. 874–880 (2009). doi:10.1038/sj.bjc.6604949

51. Dewhirst, M. W. A potential solution for eliminating hypoxia as a cause for radioresistance. *Proc. Natl. Acad. Sci. U. S. A.* **115**, 10548–10550 (2018).

52. Harris, A. L., Hochhauser, D. & Harris, A. L. MECHANISMS OF MULTIDRUG RESISTANCE IN CANCER TREATMENT. *Actu Oncol* **31**, 205–213 (1992).

53. Repository, Z. O. University of Zurich The hypoxia-inducible factor-1 alpha is a negative factor for tumor therapy The hypoxia-inducible factor-1 alpha is a negative factor for tumor therapy. **22**, (2003).

54. Alhallak, K. *et al.* Optical imaging of radiation-induced metabolic changes in radiation-sensitive and resistant cancer cells. *J. Biomed. Opt.* **22**, 60502 (2017).

55. Chung, P. *et al.* Tumor Hypoxia Predicts Biochemical Failure following Radiotherapy for Clinically Localized Prostate Cancer. **18**, 2108–2115 (2012).

56. Andrac-meyer, L. & Haddad, O. Overexpression of hypoxia-inducible factor HIF-1 a predicts early relapse in breast cancer : Retrospective study in a series of 745 patients. **739**, 734–739 (2005).

57. Powathil, G., Kohandel, M., Milosevic, M. & Sivaloganathan, S. Modeling the spatial distribution of chronic tumor hypoxia: Implications for experimental and clinical studies. *Comput. Math. Methods Med.* **2012**, (2012).

58. Lanzen, J. *et al.* Direct Demonstration of Instabilities in Oxygen Concentrations within the Extravascular Compartment of an Experimental Tumor. 2219–2224 (2006). doi:10.1158/0008-5472.CAN-03-2958

59. Nejad, E. *et al.* The role of hypoxia in the tumor microenvironment and development of cancer stem cell : a novel approach to developing treatment. *Cancer Cell Int.* 1–26 (2021). doi:10.1186/s12935-020-01719-5

60. Martinive, P. *et al.* Impact of cyclic hypoxia on HIF-1?? regulation in endothelial cells - New insights for anti-tumor treatments. *FEBS J.* (2009). doi:10.1111/j.1742-4658.2008.06798.x

61. Cooper, C. *et al.* Intermittent hypoxia induces proteasome-dependent down-regulation of estrogen receptor α in human breast carcinoma. *Clin. cancer Res.* **10**, 8720–8727 (2004).

62. Cairns, R. A. & Hill, R. P. Acute hypoxia enhances spontaneous lymph node metastasis

in an orthotopic murine model of human cervical carcinoma. *Cancer Res.* **64**, 2054 (2004).

63. Knuth, J. *et al.* Hypoxia-inducible factor-1α activation in HPV-positive head and neck squamous cell carcinoma cell lines. *Oncotarget* **8**, 89681–89691 (2017).

64. Lee, D. E. *et al.* A Radiosensitizing Inhibitor of HIF-1 alters the Optical Redox State of Human Lung Cancer Cells In Vitro. *Sci. Rep.* **8**, 8815 (2018).

65. Hsu, P. P. & Sabatini, D. M. Cancer cell metabolism: Warburg and beyond. *Cell* (2008). doi:10.1016/j.cell.2008.08.021

66. Bottaro, Larsen, B. 基因的改变NIH Public Access. *Bone* **23**, 1–7 (2008).

67. Kaelin, W. G. & Thompson, C. B. Q and A: Cancer: clues from cell metabolism. *Nature* **465**, 562–564 (2010).

68. Ferreira, L. M. R. Cancer metabolism: The Warburg effect today. *Experimental and Molecular Pathology* (2010). doi:10.1016/j.yexmp.2010.08.006

69. Bottaro, Larsen, B. 基因的改变NIH Public Access. *Bone* **23**, 1–7 (2008).

70. Neagu, M. *et al.* Inflammation and metabolism in cancer cell—mitochondria key player. *Front. Oncol.* **9**, 1–15 (2019).

71. Lewis, C. A. *et al.* Tracing Compartmentalized NADPH Metabolism in the Cytosol and Mitochondria of Mammalian Cells. *Mol. Cell* **55**, 253–263 (2014).

72. Li, C. & Jackson, R. M. Reactive species mechanisms of cellular hypoxia-reoxygenation injury. *AJP Cell Physiol.* (2002). doi:10.1152/ajpcell.00112.2001

73. Pan, X. *et al.* Increased unsaturation of lipids in cytoplasmic lipid droplets in DAOY cancer cells in response to cisplatin treatment. *Metabolomics* **9**, 722–729 (2013).

74. Lee, M. *et al.* Targeting STAT3 and oxidative phosphorylation in oncogene-addicted tumors. *Redox Biol.* **25**, 101073 (2019).

75. Heikal, A. A. Intracellular coenzymes as natural biomarkers for metabolic activities and mitochondrial anomalies. *Biomark. Med.* (2010). doi:10.2217/bmm.10.1

76. CHANCE, B. & BALTSCHEFFSKY, H. Respiratory enzymes in oxidative phosphorylation. VII. Binding of intramitochondrial reduced pyridine nucleotide. *J. Biol. Chem.* **233**, 736–739 (1958).

77. Chance, B., Cohen, P., Jobsis, F. & Schoen, B. Intracellular Oxidatior Reduction States in VivI The microfluorometry of pyridine nucleotide givi a continuous measurement of the oxidation stat. **137**, (1962).

78. Scholz, R., Thurman, R. G., Williamson, J. R., Chance, B. & Bücher, T. Flavin and pyridine nucleotide oxidation-reduction changes in perfused rat liver. I. Anoxia and subcellular localization of fluorescent flavoproteins. *J. Biol. Chem.* **244**, 2317–2324

(1969).

79. Xu, H. N., Hall, B. B., Glickson, J. D., Chance, B. & Li, L. Z. Quantitative mitochondrial redox imaging of breast cancer metastatic potential. **15**, 1–10 (2010).

80. Mayer, J. G.-. Von M a r i a G 6 p p e r t - M a y e r. **114**, (1928).

81. Mayer, A. *et al.* **双光子激光**扫描荧光显微术. 1–4 (1990).

82. Benninger, R. K. P. & Piston, D. W. *Two-photon excitation microscopy for unit 4.11 the study of living cells and tissues*. *Current Protocols in Cell Biology* (2013). doi:10.1002/0471143030.cb0411s59

83. Georgakoudi, I. & Quinn, K. P. Optical Imaging Using Endogenous Contrast to Assess Metabolic State. *Annu. Rev. Biomed. Eng.* (2012). doi:10.1146/annurev-bioeng-071811-150108

84. Quinn, K. P. *et al.* Characterization of metabolic changes associated with the functional development of 3D engineered tissues by non-invasive, dynamic measurement of individual cell redox ratios. *Biomaterials* (2012). doi:10.1016/j.biomaterials.2012.04.024

85. Quinn, K. P. *et al.* Quantitative metabolic imaging using endogenous fluorescence to detect stem cell differentiation. *Sci. Rep.* (2013). doi:10.1038/srep03432

86. Alhallak, K., Rebello, L. G., Muldoon, T. J., Quinn, K. P. & Rajaram, N. Optical redox ratio identifies metastatic potential-dependent changes in breast cancer cell metabolism. *Biomed. Opt. Express* **7**, (2016).

87. Pouli, D. *et al.* Label-free, High-Resolution Optical Metabolic Imaging of Human Cervical Precancers Reveals Potential for Intraepithelial Neoplasia Diagnosis. *Cell Reports Med.* **1**, 100017 (2020).

88. Waks, A. G. & Winer, E. P. Breast Cancer Treatment: A Review. *JAMA - J. Am. Med. Assoc.* **321**, 288–300 (2019).

89. Thrivehive.com. Questions to ask about your competitors. 2–3 (2019).

90. Brindle, K. New approaches for imaging tumour responses to treatment. *Nat. Rev. Cancer* **8**, 94–107 (2008).

91. Lindner, J. R. Molecular imaging with contrast ultrasound and targeted microbubbles. *J. Nucl. Cardiol.* **11**, 215–221 (2004).

92. Roblyer, D. *et al.* Optical imaging of breast cancer oxyhemoglobin flare correlates with neoadjuvant chemotherapy response one day after starting treatment. *Proc. Natl. Acad. Sci. U. S. A.* **108**, 14626–14631 (2011).

93. Telle, H. H. & Ureña, Á. G. *Diffuse Optical Imaging*. *Laser Spectroscopy and Laser Imaging* (2019). doi:10.1201/9781315156989-20

94. Bensinger, S. J. & Christofk, H. R. New aspects of the Warburg effect in cancer cell

biology. *Seminars in Cell and Developmental Biology* (2012). doi:10.1016/j.semcdb.2012.02.003

95. Pavlova, N. N. & Thompson, C. B. The Emerging Hallmarks of Cancer Metabolism. *Cell Metabolism* (2016). doi:10.1016/j.cmet.2015.12.006

96. Kolenc, O. I. & Quinn, K. P. Evaluating cell metabolism through autofluorescence imaging of NAD(P)H and FAD. *Antioxidants Redox Signal.* **30**, 875–889 (2019).

97. Aon, M. A., Cortassa, S., Marbán, E. & O'Rourke, B. Synchronized Whole Cell Oscillations in Mitochondrial Metabolism Triggered by a Local Release of Reactive Oxygen Species in Cardiac Myocytes. *J. Biol. Chem.* **278**, 44735–44744 (2003).

98. Ostrander, J. H. *et al.* Optical redox ratio differentiates breast cancer cell lines based on estrogen receptor status. *Cancer Res.* (2010). doi:10.1158/0008-5472.CAN-09-2572

99. Walsh, A. J. *et al.* Optical Metabolic Imaging Identi fi es Glycolytic Levels , Subtypes , and Early-Treatment Response in Breast Cancer. **73**, 14–18 (2013).

100. Walsh, A. *et al.* Optical imaging of metabolism in HER2 overexpressing breast cancer cells References and Links. *Biomed. Opt. EXPRESS J. Med* **3**, 1659–1672 (2520).

101. Alhallak, K., Rebello, L. & Rajaram, N. Optical imaging of cancer cell metabolism in murine metastatic breast cancer. in *Optics InfoBase Conference Papers* (2014). doi:10.1364/CANCER.2016.JM3A.34

102. Shah, A. T. *et al.* Optical Metabolic Imaging of Treatment Response in Human Head and Neck Squamous Cell Carcinoma. **9**, (2014).

103. Shah, A. T., Heaster, T. M. & Skala, M. C. Metabolic imaging of head and neck cancer organoids. *PLoS One* **12**, 1–17 (2017).

104. Bischel, L. L., Beebe, D. J. & Sung, K. E. Microfluidic model of ductal carcinoma in situ with 3D, organotypic structure. *BMC Cancer* **15**, 1–10 (2015).

105. Ayuso, J. M. *et al.* Organotypic microfluidic breast cancer model reveals starvation-induced spatial-temporal metabolic adaptations. *EBioMedicine* **37**, 144–157 (2018).

106. Gil, D. A., Deming, D. & Skala, M. C. Patient-derived cancer organoid tracking with wide-field one-photon redox imaging to assess treatment response. *J. Biomed. Opt.* **26**, 1–19 (2021).

107. Rubart, M. *et al.* Physiological coupling of donor and host cardiomyocytes after cellular transplantation. *Circ. Res.* **92**, 1217–1224 (2003).

108. Jones, J. S., Small, D. M. & Nishimura, N. In vivo calcium imaging of cardiomyocytes in the beating mouse heart with multiphoton microscopy. *Front. Physiol.* **9**, 1–13 (2018).

109. Rubart, M. Two-photon microscopy of cells and tissue. *Circ. Res.* **95**, 1154–1166 (2004).

Chapter 1: Appendix

In 2020, nearly 1,806,590 new cases of cancer were diagnosed in the United States. Radiation and/or chemotherapy is the primary form of treatment in a majority of cancer patients. A critical challenge encountered by these patients is treatment resistance. While there is a large body of knowledge suggesting that tumor hypoxia (lack of oxygen) is responsible for treatment resistance and has been directly linked to metastases, the role of metabolic changes within cancer cells that may contribute to treatment resistance and tumor metastases are not well understood. *The overall goal of this dissertation is to study the effects of microenvironmental stresses induced by hypoxia and radiation on tumor cell metabolism using nondestructive and label-free optical imaging.*

Optical imaging based on two-photon excited fluorescence (TPEF) can provide a quantitative measure of cellular metabolism by imaging the endogenous fluorophores – Nicotinamide Adenine Dinucleotide (NADH) and Flavin Adenine Dinucleotide (FAD). The optical redox ratio (ORR) of FAD/(NADH+FAD) has been used to investigate changes in cell metabolism during cell differentiation and malignant transformation *in vitro* and *in vivo*. Furthermore, the ORR has been used to monitor treatment response in tumor organoids from different organ sites. The central premise of this dissertation is that the ORR can be utilized to determine the metabolic changes in response to microenvironmental stresses in tumors. We propose the following specific aims:

Aim 1: Determine the metabolic effects of chronic and intermittent hypoxia in murine breast cancer cells and its association with metastatic potential.

While several studies have investigated the effects of hypoxia on metabolism, hypoxia in tumors is not static. Rather, variations in blood flow cause cancer cells within and at the oxygen diffusion limit to experience cycles of hypoxia or intermittent hypoxia. Using a panel of isogenic murine breast cancer cells of different metastatic potential, we will test the hypothesis that

chronic and intermittent hypoxia leads to cell-line specific changes in ORR which can be associated with metastatic potential. At the end of this aim, we will determine the distinct longitudinal changes in optical redox ratio within each cell line in response to chronic and intermittent hypoxia. We will also determine if such changes can be directly correlated with metastatic potential through specific targeting of metastasis-promoting genes.

Aim 2: Determine the effects of radiation therapy on cellular metabolism in a panel of radiation-sensitive and resistant human head and neck cancer cells.

Previous studies have determined the negative effects of tumor hypoxia on the responsiveness of chemotherapy and radiation in tumors; however, our understanding of the effects of radiation therapy on cellular metabolism is limited. We will evaluate longitudinal changes in cellular metabolism in response to radiation therapy in a group of radiation-resistant and radiation-sensitive cell lines. The radiation sensitivity of these cell lines has been established previously. We will test the hypothesis that exposure to radiation therapy will reveal distinct metabolic changes in ORR that can be associated with radiation resistance or sensitivity. We will also determine whether hypoxia-inducible factor (HIF-1) plays a key role in mediating treatment resistance in these cancer cells.

Aim 3: Evaluate the changes in cellular metabolism associated with acquisition of treatment resistance.

In this Aim, we will evaluate the effects of radiation therapy on cellular metabolism in a panel of isogenic cell lines that have been engineered to have increasing levels of radiation resistance. These studies will allow us to understand metabolic reprogramming associated with radiation resistance in a panel of cell lines with a common genetic background. We will also determine the role of HIF-1 in the development of radiation resistance by measuring metabolic changes in response to HIF-1 inhibition in these cell lines.

Chapter 2:

Optical metabolic imaging of the effects of chronic and intermittent hypoxia in murine breast cancer cells

1. Introduction

Tumor hypoxia has been associated with poor disease-free survival, resistance to radiation therapy and the development of distant metastasis in multiple organ sites. Cancer cells frequently outgrow their vascular supply, resulting in regions of hypoxia within a tumor. While increased oxygen consumption and the oxygen diffusion limit can contribute to the development of such chronically hypoxic regions within a tumor, the irregular development of tumor vasculature can also lead to temporal variations in hypoxia. Specifically, variations in red cell flux through poorly developed vessels leads to fluctuations in oxygen availability to the cells. Such fluctuations can cause tumor cells within and at the oxygen diffusion limit in tumors to experience cycles of hypoxia[1,2,3,4,5,6]. The periodicity of such fluctuations has been measured to be on the order of minutes to days[3,4,7,8,9] . Exposure to such intermittent or cycling hypoxia (IH) has been shown to increase the number of breast cancer stem cells[10], downregulate estrogen receptor (Erα)[11] , increase radiation resistance *in vitro*[12] , increase DNA damage[13] , and increase metastatic potential both in vitro and in *vivo*[14,15,16] , all relative to chronic hypoxia. Reoxygenation following acute hypoxia results in the generation of reactive oxygen species that can cause DNA damage. Pires et al. have demonstrated that cells with a p53 mutation are able to restart replication and continue proliferation in the presence of ROS-induced DNA damage caused by reoxygenation events following short periods of hypoxia. ROS have also been shown to be sufficient and necessary for stabilization of HIF-1. These cycles of hypoxia-reoxygenation can lead to upregulation of hypoxia-inducible factor (HIF-1α) to a level greater than that caused

by chronic hypoxia. HIF-1 is a master regulator of oxygen homeostasis and is known to affect more than 100 metabolic genes. While researchers have studied the effects of normoxia and chronic hypoxia on glucose consumption and lactate production to examine the 'Warburg effect[17,18], few studies have compared the metabolic consequences of cycling hypoxia and chronic hypoxia.

Optical imaging of endogenous fluorescence from the metabolic cofactors, nicotinamide adenine dinucleotide (NADH) and flavin adenine dinucleotide (FAD) can provide a quantitative measure of the redox status of a cell. The optical redox ratio of FAD/FAD+NADH is strongly correlated with mass spectrometry-based measurements of the concentrations of NAD+/NADH and can be used to determine metabolic changes within a cell. Specifically, a decrease in the optical redox ratio can be attributed to hypoxia, fatty acid synthesis or fatty acid oxidation while an increase in the redox ratio can be associated with increased oxidative metabolism or glucose starvation.

Using the optical redox ratio, we have shown that radiation therapy causes a significant decrease in the optical redox ratio of lung cancer cells, concordant with a significant increase in HIF-1 expression[19]. We have also shown that HIF-1 inhibition increases the optical redox ratio, and that this was associated with a decrease in pyruvate dehydrogenase kinase (PDK-1), which inhibits pyruvate entry to the mitochondria and an increase in ROS[20]. These studies have demonstrated the sensitivity of the optical redox ratio to modulation of pathways involved in the hypoxic response of a cancer cell.

In a recent study on a panel of breast cancer cell lines with the same genetic background (all derived from the same murine tumor), we found that exposure to a short duration of hypoxia followed by reoxygenation (1 hour each) resulted in a metastatic potential-dependent change in the optical redox ratio[21]. We found a significant increase in the optical redox ratio in the highly metastasis-capable 4T1 and 4T07 cell lines after reoxygenation following hypoxia compared with normoxic control and no change in the non-metastatic 168FARN and 67NR cell lines.

Previous work has shown that the differences in metastatic potential of these cell lines was likely due to TWIST, a master regulator of embryonic morphogenesis[22]. To investigate whether the differences in the optical redox ratio observed in our previous study were due to TWIST, we used CRISPR/Cas9 gene editing to delete TWIST in the 4T1 cell line and performed optical imaging of the cellular redox state on this clonal population. We compared the metabolic effects of exposure to 3 hours of chronic or cycling hypoxia in the 4T1-TWIST$^{-/-}$, parental 4T1, 168FARN, and 66cl4. We found a significant increase in the optical redox ratio only in poorly metastatic 168FARN cells after exposure to chronic hypoxia. The duration of chronic hypoxia and frequency of intermittent hypoxia utilized in this study did not result in significant metabolic differences between the two types of hypoxia. This can be attributed to hypoxic cycles with oxygen levels set at 21% for normoxia and 0.5% for hypoxia as compared to *invivo* settings wherein the oxygen levels for hypoxia would be less than 5%while oxygen levels for normoxia would be around 5%. While deletion of TWIST did result in lower redox ratio compared with the parental 4T1 cell line, this was not statistically significant. Further work utilizing longer durations of hypoxia, varying cycles of intermittent hypoxia, and imaging during hypoxia is necessary to better capture the metabolic differences between the two types of hypoxia.

2. Methods

2.1 Cell Culture

The cell lines used in this study – 4T1, 168FARN and 66cl4 – were first developed from a spontaneous breast tumor in a BALB/c mouse and were provided by Dr. Fred Miller from Karmanos Cancer Institute. 4T1-Twist$^{-/-}$ was developed using CRISPR-cas9 gene editing techniques. Cells were cultured using Dulbecco's Modified Eagle's Medium (DMEM) supplemented with 10%(v/v) of Fetal Bovine Serum (FBS), 2 mM L-Glutamine, 1% (v/v) nonessential amino acids, and 1%(v/v) penicillin-streptomycin in a humidified incubator that was

set to 5% CO_2 and 37℃. Cells were passaged when they reached about 80% confluency and were utilized for all the experiments in the first 10 passages.

2.2 CRISPR/Cas9 Deletion of TWIST and Clonal Selection

Using the sgRNA guide tool provided by the Zhang laboratory (MIT, Cambridge, MA), the 20-base pair sgRNA was identified to target the TWIST gene, also known as the Twist1 gene, in 4T1 mouse cells. The sgRNA was cloned into pCas-Guide-EF1a-GFP plasmids (Origene, Rockville, MD) These plasmids were expanded using E. Coli bacteria, and plasmid isolation from E. Coli was achieved using the QIAGEN Plasmid Maxi Kit. For plasmid transfection, 4T1 cells were seeded in a 6-well plate at a concentration of one million cells/well and incubated for 24 hours. 10 µg of plasmid were added to Lipofectamine 3000 and added to the 4T1 cells. After 24 to 48 hours, green fluorescent protein (GFP) signal was detected using a Nikon TiE fluorescence microscope workstation with a CoolSnap HQ2 camera; signals exhibiting GFP expression indicated the transfected cells, as the plasmid contained GFP. Transfected 4T1 cells were suspended in a PBS solution at a concentration of two million cells per ml. The transfected cells were filtered through a 50 µm filter into a FACS tube. Cell sorting was achieved through the FACS Aria III System (BD Biosciences, San Jose, CA). The 5% of transfected cells that exhibited the greatest GFP expression were sorted to have cells with the highest CRIPSR/Cas9 plasmid concentration. The sorted cells were incubated and cultured for 7 to 14 days in the same incubation settings described above. The cell colonies were then cloned into 13 clones to produce a population that had the least TWIST expression, as confirmed through Western blot.

2.3 Exposure to Hypoxia

A dual gas controller (Oxycycler C42, Biospherix, Parish, NY) connected to a modular sub-chamber was used to control oxygen, nitrogen, and carbon dioxide levels. The modular sub-chamber is placed inside a humidified incubator with temperature set at 37°C, 5% CO_2 which

houses the experimental cell plates. The gas controller is located outside the incubator and is connected to the sub-chamber through the door of the incubator. For chronic hypoxia, the gas controller was set to a constant level of 0.5% O_2 and 5% CO_2 for a period of 3 hours. The controller reaches the set point of 0.5% O_2 in approximately 20 minutes. Hypoxic exposure of cells did not include this 20-minute-period. For intermittent hypoxia, the 3 hours of hypoxic exposure was delivered over a period of 6 hours with 1-hour intervening periods of reoxygenation at 21% O_2. The time required for oxygen levels to adjust from 0.5% to 21% and vice versa was taken into consideration and was accounted in the timeframes. A detailed schematic of chronic and intermittent hypoxia exposure is presented in Figure 1.

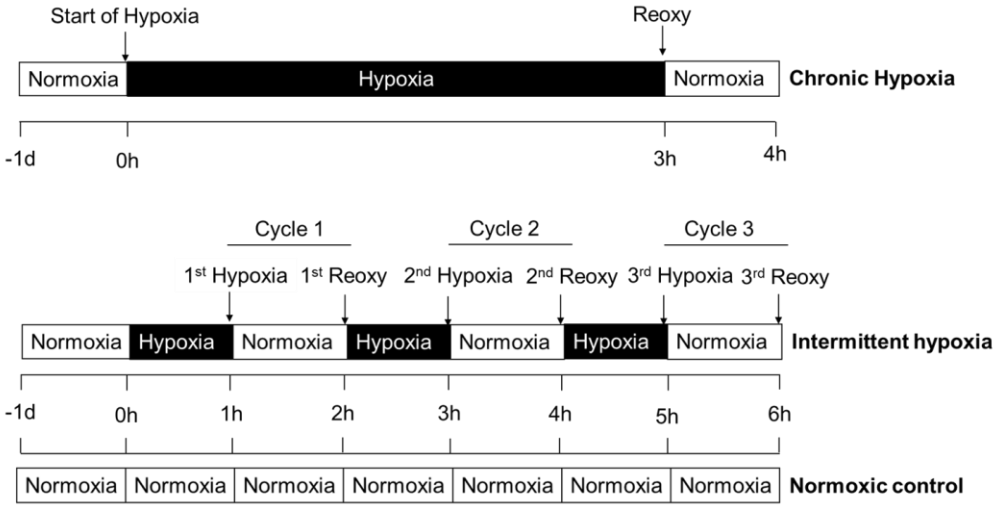

Figure 1. Experimental set up of chronic hypoxia and intermittent or cyclic hypoxia along with the normoxic control.

2.4 Two-photon imaging of cellular autofluorescence

Cells were plated on a glass slide at a pre-determined cellular density in a standard 6-well plate on the day prior to experiment. After 24 hours, the glass slide was removed and was placed in a heated chamber (37˚C) perfused with 1 ml of regular DMEM media. Cells were imaged using a

custom-built resonant-scanning multiphoton microscope with a MaiTai ultrafast Ti:Sapphire tunable laser source (Spectra Physics, Santa Clara, CA). For NADH fluorescence, the laser source was excited at 750nm and 860nm for FAD fluorescence. Image acquisition was executed employing non-descanned GaAsP photomultiplier tubes (H7422-40, Hamamatsu) with 460/40 nm (NADH) or 525/40 nm (FAD) bandpass filters, respectively. Images (512 x 512 pixels; 16-bit depth; 130 µm x 130 µm) were acquired using a 20x water immersion objective (NA = 0.8, working distance = 3.5 mm, diffraction-limited lateral resolution = 0.6 µm). Image analysis was accomplished using MATLAB.

The optical redox ratio images were generated by computing pixel wise ratios of FAD/(NADH+FAD) fluorescence. For data presentation and statistical analysis, the average redox ratios of the cell plates were calculated by separately quantifying the average FAD and NADH intensities from the respective images and taking the ratio of these values. For each cell line, distinct cell plates were imaged at normoxia and post hypoxia for each time point, for both chronic and intermittent hypoxia. Three fields of view were acquired in each cell plate and 6 cells were randomly selected within each field of view. Two independent runs of these experiments were performed. An in-depth schematic of chronic and intermittent hypoxia exposure is presented in Figure 2.

2.5 Statistical analysis

A nested, two-way analysis of variance (ANOVA) was used to determine statistically significant differences in the average redox ratio. Cell line and the hypoxic perturbation (intermittent or chronic) were considered fixed effects while the cell plates and fields of view nested within each group were considered random effects. Interactions between all effects were also considered. Post-hoc Tukey HSD tests were used to evaluate statistical significance between specific cell groups.

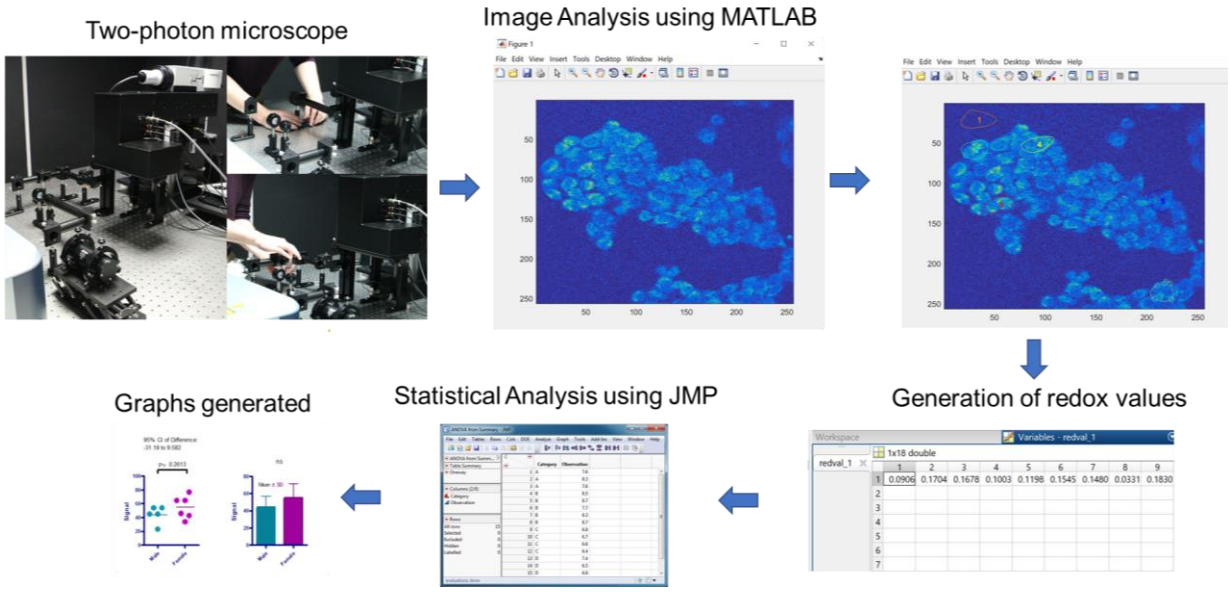

Figure 2. Data acquisition and analysis workflow using two-photon microscope and MATLAB.

3. Results

3.1. Exposure to chronic hypoxia leads to a significant increase in the optical redox ratio only in poorly metastatic 168FARN cells

We exposed the cells to chronic hypoxia for 3 hours at 0.5% O_2 and acquired NADH and FAD fluorescence images at normoxia (no hypoxic exposure) and 0-, 60-, and 120-min post hypoxia. Representative images at each time point from each cell line are shown in Figure 3A. We found no significant changes in the optical redox ratio of the 4T1 cell line at 0, 60, and 120 post-hypoxic exposure. While the 4T1-Twist$^{-/-}$ cells had a lower optical redox ratio under normoxic conditions compared with the 4T1 cell line, exposure to chronic hypoxia did not cause a significant change in the optical redox ratio in 4T1-Twist$^{-/-}$ cells at any of the time points examined. In contrast, the optical redox ratio was higher in 168FARN cells examined immediately after hypoxia ($p > 0.05$) and nearly twice that of the normoxic control after 60 minutes of reoxygenation following hypoxia ($p = 0.01$). At 120 minutes post hypoxia, the optical redox ratio was significantly lower than the 60-minute time point ($p = 0.027$). and had declined

to the level of normoxic control. Finally, the 66cl4 cells had the highest optical redox ratio under normoxic conditions of all the cell lines examined and were significantly higher than the 4T1 and 168FARN cells ($p = 0.004$). Similar to the 4T1 and 4T1-Twist $^{-/-}$ cells, the 66cl4 cells did not show significant changes in the ORR upon exposure to chronic hypoxia

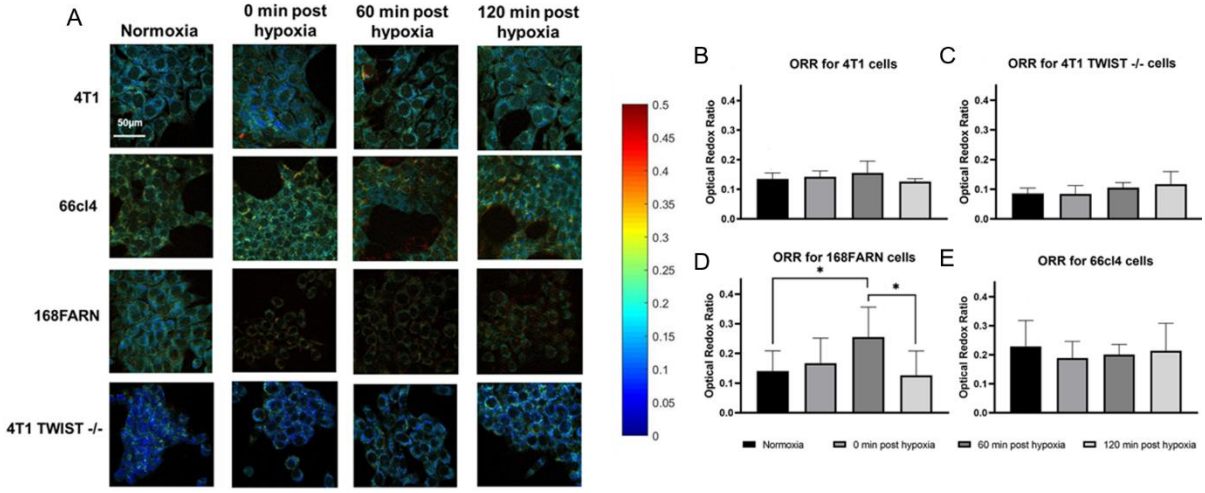

Figure 3. Exposure to chronic hypoxia causes a significant change in the optical redox ratio of only poorly metastatic 168FARN cells. A. Representative redox ratio images of 4T1, 66cl4, 168FARN and 4T1-Twist$^{-/-}$ under normoxia and 0-, 60-, and 120-min post chronic hypoxia. We recorded 18 images for each of the time points mentioned above, the images provided represent the fields if view with redox ratios closest to the average of the 18 fields of view together. Quantification of mean redox ratios for B. 4T1, C. 4T1-Twist$^{-/-}$, D. 168FARN and E. 66cl4 cells under normoxia, and 0-, 60-, and 120-min post hypoxia. The seeding density for each cell line was individually optimized before the actual experiments. Experiments were performed in triplicate across 2 independent experiments. Error bars represent standard deviation of the mean, n=2. Asterisks placed above bars indicate statistical significance.
* Denotes statistical significance at $p<0.05$.

3.2. Exposure to intermittent hypoxia does not lead to changes in the optical redox ratio of metastatic and non-metastatic cancer cells

We studied the metabolic effects of intermittent hypoxia by delivering the 3 total hours of hypoxia in cycles of 1 hour (alternating with 1 hour of reoxygenation). Figure 3A shows representative images from each cell line that were acquired 60 minutes after completion of intermittent hypoxia and their respective normoxic controls. 4T1-Twist$^{-/-}$, 168FARN and 66cl4 cells show a small but insignificant increase in the optical redox ratio at 60-min post hypoxia as

compared to their normoxic controls. However, there was a small decrease in the optical redox ratio of the 4T1 cells.

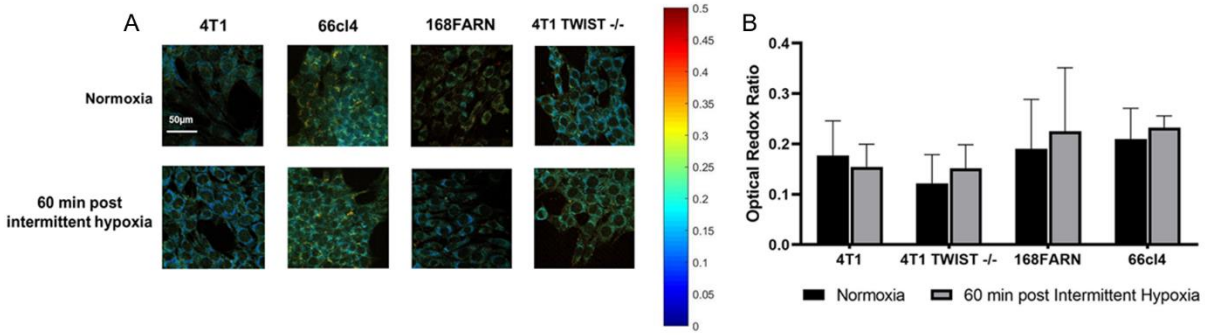

Figure 4. Intermittent hypoxia does not cause a significant change in the optical redox ratio. A Representative redox ratio images of 4T1, 66cl4, 168FARN and 4T1-TWIST -/- under normoxia and 60 min post intermittent hypoxia. We recorded 18 images for each of the time points mentioned above, the images provided represent the fields if view with redox ratios closest to the average of the 18 fields of view together. B. Quantification of mean redox ratios of 4T1, 4T1-TWIST -/-, 168FARN and 66cl4 60 min post chronic and intermittent hypoxia. The seeding density for each cell line was individually optimized before the actual experiments. Experiments were performed in triplicate across 2 independent experiments. Error bars represent standard deviation of the mean, n=2.

3.3. There are no differences in the metabolic response to 3 hours of chronic or intermittent hypoxia in glycolytic murine breast cancer cells.

We calculated the difference in the redox ratio between the post-hypoxia and corresponding normoxia groups for each cell line. We found no differences in the magnitude of change of the optical redox ratio in response to chronic or intermittent hypoxia. The magnitude of change also does not appear to depend on the metastatic potential of the cell line.

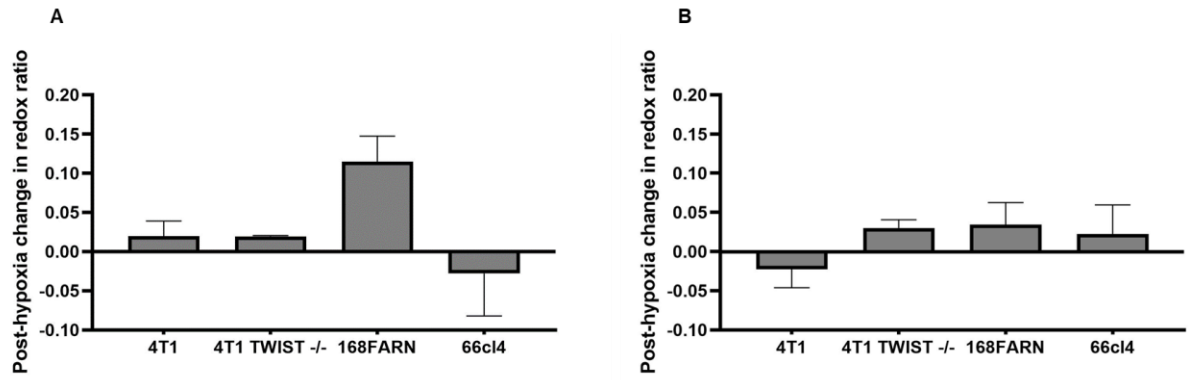

Figure 5. We observe no significant differences in optical redox ratio after exposure to 3 hours of chronic and intermittent hypoxia. Bar plots represent the difference in the mean values of normoxia and post-hypoxia reoxygenation groups on exposure to A. chronic hypoxia and B. Intermittent hypoxia. Error bars represent standard deviation and were calculated as follows: $\sqrt{(\boldsymbol{sd_1})^2 + (\boldsymbol{sd_2})^2}$, where sd_1 and sd_2 represent the normoxia and post-hypoxia groups within each cell line.

4. Discussion

Hypoxia and metabolic reprogramming have been independently shown to be key determinants of cancer cell metastasis. While a clear difference in tumor fate has been demonstrated for chronic and intermittent hypoxia, there are few studies that have explored the metabolic changes associated with each type of hypoxia and whether such metabolic changes are ultimately responsible for promoting cancer cell metastasis. This study uses label-free and non-destructive imaging of NADH and FAD autofluorescence to compare metabolic changes in response to each type of hypoxia in cell lines of known metastatic potential.

Previously, many studies have used hypoxic fractions ranging from minutes to hours to days. An earlier study from our lab[21] had shown that the optical redox ratio of murine breast cancer cells at baseline decreased with decreasing metastatic potential (4T1>4T07>168FARN) after exposure to 60 minutes of hypoxia. Using this as a motivation, we decided to test our cells to higher hypoxic fractions by exposing our cells to 3 hours of hypoxia. Here, we found that the baseline redox ratio was nearly unchanged across all cell lines, except for the 66cl4 cells that had a redox ratio significantly higher than the 4T1 cells ($p < 0.05$). While both 4T1 and 66cl4 cells are highly

metastatic, the 4T1 cells metastasize through the vasculature while the 66cl4 cells are more likely to metastasize through the draining lymph nodes[23]. This downward shift in the redox ratio of the 4T1 cells compared to the previous study (0.4 vs. 0.14) could be attributed to a higher passage number for these cells. Repeated passaging of cells in high-glucose medium has the potential to render these cells more glycolytic, which is reflected in the lower redox ratio. In accordance with this shift towards increased glycolysis, the 4T1 cells showed no significant change in the redox ratio in response to 3 hours of chronic or intermittent hypoxia. On the other hand, our previous study had found an increase in the redox ratio of highly metastatic cancer cells (4T1 and 4T07) after exposure to just 60 minutes of hypoxia. A lack of metabolic response to hypoxic perturbations is representative of aerobic glycolysis. Previous studies in human breast cancer cells have shown no change in glucose consumption or lactate production of malignant MDA-MB-231 cells in response to hypoxia while a significant increase in both parameters was observed in the benign MCF7 cells[17]. We observe similar results here, with the poorly metastatic 168FARN cells showing a statistically significant increase in the redox ratio upon exposure to chronic hypoxia. While there was a general trend towards an increase in the redox ratio after intermittent hypoxia in all cell lines, these changes were not statistically significant. Exposure to intermittent hypoxia has been shown to lead to the generation of ROS[13]. In addition, we have demonstrated an increase in the redox ratio concordant with an increase in ROS[20]. Further studies evaluating the levels of mitochondrial ROS are necessary to determine if the changes in the redox ratio observed here are due to an increase in ROS.

To determine if our previous results demonstrating a metastatic potential-dependent change in the optical redox ratio were due to the TWIST gene, we investigated the effect of deleting TWIST from the 4T1 cell line on the optical redox ratio. We observed a decrease in the baseline optical redox ratio of the 4T1-TWIST$^{-/-}$ cells compared with the parental 4T1 cells and there were no differences between the cell lines in their response to chronic and intermittent hypoxia. Another study has shown that overexpression of TWIST in MCF10A mammary epithelial

cells led to an increase in glycolysis and hence lactate production at baseline and in response to hypoxia[24]. Given these results, it is necessary to investigate the effects of TWIST expression on cellular metabolism in multiple cell lines.

In summary, we have used two-photon imaging of cellular metabolism to compare the metabolic response to chronic and intermittent hypoxia. While our data do not reveal differences in the metabolic response to each type of hypoxia, it is important to note that the changes in cellular metabolism are highly dependent on the duration of hypoxia and the number of hypoxia-reoxygenation cycles. Additionally, because we perform imaging in the reoxygenation period following hypoxia, these data do not provide a clear picture of the cell's metabolic response during hypoxia. Optical metabolic imaging in response to longer durations of hypoxia as well as *during* hypoxia can better elucidate the metabolic differences between chronic and intermittent hypoxia.

References:

1. Chaplin, D. J., Olive, P. L. & Durand, R. E. Intermittent blood flow in a murine tumor: radiobiological effects. *Cancer Res.* **47**, 597–601 (1987).

2. Chaplin, D. J., Durand, R. E. & Olive, P. L. Acute hypoxia in tumors: implications for modifiers of radiation effects. *Int. J. Radiat. Oncol. Biol. Phys.* **12**, 1279–1282 (1986).

3. Kimura, H. *et al.* Fluctuations in red cell flux in tumor microvessels can lead to transient hypoxia and reoxygenation in tumor parenchyma. *Cancer Res.* **56**, 5522–5528 (1996).

4. Lanzen, J. *et al.* Direct Demonstration of Instabilities in Oxygen Concentrations within the Extravascular Compartment of an Experimental Tumor. 2219–2224 (2006). doi:10.1158/0008-5472.CAN-03-2958

5. Cárdenas-Navia, L. I. *et al.* The pervasive presence of fluctuating oxygenation in tumors. *Cancer Res.* **68**, 5812–5819 (2008).

6. Dewhirst, M. W., Cao, Y. & Moeller, B. Cycling hypoxia and free radicals regulate angiogenesis and radiotherapy response. *Nature Reviews Cancer* (2008). doi:10.1038/nrc2397

7. Baudelet, C. *et al.* Physiological noise in murine solid tumours using T2*-weighted gradient-echo imaging: a marker of tumour acute hypoxia? *Phys. Med. Biol.* **49**, 3389 (2004).

8. Braun, R. D., Lanzen, J. L. & Dewhirst, M. W. Fourier analysis of fluctuations of oxygen tension and blood flow in R3230Ac tumors and muscle in rats. *Am. J. Physiol. Circ. Physiol.* **277**, H551–H568 (1999).

9. Yu, B. *et al.* Measuring tumor cycling hypoxia and angiogenesis using a side-firing fiber optic probe. *J. Biophotonics* **7**, 552–564 (2014).

10. Louie, E. *et al.* Identification of a stem-like cell population by exposing metastatic breast cancer cell lines to repetitive cycles of hypoxia and reoxygenation. *Breast Cancer Res.* (2010). doi:10.1186/bcr2773

11. Cooper, C. *et al.* Intermittent hypoxia induces proteasome-dependent down-regulation of estrogen receptor α in human breast carcinoma. *Clin. cancer Res.* **10**, 8720–8727 (2004).

12. Martinive, P. *et al.* Preconditioning of the tumor vasculature and tumor cells by intermittent hypoxia: Implications for anticancer therapies. *Cancer Res.* (2006). doi:10.1158/0008-5472.CAN-06-2056

13. Pires, I. M. *et al.* Effects of acute versus chronic hypoxia on DNA damage responses and genomic instability. *Cancer Res* **70**, 925–935 (2010).

14. Cairns, R. A. & Hill, R. P. Acute hypoxia enhances spontaneous lymph node metastasis in an orthotopic murine model of human cervical carcinoma. *Cancer Res.* **64**, 2054 (2004).

15. Cairns, R. A., Kalliomaki, T. & Hill, R. P. *Acute (Cyclic) Hypoxia Enhances Spontaneous Metastasis of KHT Murine Tumors 1*. *CANCER RESEARCH* **61**, (2001).

16. Dai, Y., Bae, K. & Siemann, D. W. Impact of hypoxia on the metastatic potential of human prostate cancer cells. *Int. J. Radiat. Oncol. Biol. Phys.* **81**, 521–528 (2011).

17. Gillies, R. J., Robey, I. & Gatenby, R. A. Causes and Consequences of Increased Glucose Metabolism of Cancers. *J. Nucl. Med.* (2008). doi:10.2967/jnumed.107.047258

18. Robey, I. F., Lien, A. D., Welsh, S. J., Baggett, B. K. & Gillies, R. J. Hypoxia-inducible factor-1 and the glycolytic phenotype in tumors. *Neoplasia (New York, NY)* **7**, 324 (2005).

19. Alhallak, K. *et al.* Optical imaging of radiation-induced metabolic changes in radiation-sensitive and resistant cancer cells Optical imaging of radiation-induced metabolic changes in radiation-sensitive and resistant cancer cells. doi:10.1117/1.JBO.22.6.060502

20. Lee, D. E. *et al.* A Radiosensitizing Inhibitor of HIF-1 alters the Optical Redox State of Human Lung Cancer Cells In Vitro. *Sci. Rep.* **8**, 8815 (2018).

21. Alhallak, K. *et al.* Optical redox ratio identifies metastatic potential-dependent changes in breast cancer cell metabolism. *Clin. Oncol* **34**, 2303–2311 (2016).

22. Yang, J. *et al.* Twist, a master regulator of morphogenesis, plays an essential role in tumor metastasis. *Cell* **117**, 927–939 (2004).

23. Aslakson, C. J. & Miller, F. R. Selective Events in the Metastatic Process Defined by Analysis of the Sequential Dissemination of Subpopulations of a Mouse Mammary Tumor. *Cancer Res.* **52**, 1399–1405 (1992).

24. Yang, L. *et al.* Twist promotes reprogramming of glucose metabolism in breast cancer cells through PI3K/AKT and p53 signaling pathways. *Oncotarget* (2015). doi:10.18632/oncotarget.4697

Chapter 3:

Optical metabolic imaging of the effects of radiation in head and neck cancer cells

1. Introduction:

Head and neck cancer constitutes a diverse tumor population originating from various organs like the upper aerodigestive tract, paranasal sinuses, and salivary and thyroid glands[1]. An interdisciplinary approach consisting of surgery followed by radiotherapy are the main approaches employed to combat head and neck cancers[2]. Resistance to radiation therapy is the leading cause of treatment failure in head and neck cancer therapies. One of the factors that causes impediment to radiation therapy is tumor hypoxia considering DNA damage in cells depends on existence of oxygen leading to reduced control of tumor growth and survival[3]. Radiation-induced reoxygenation in cancer cells can lead to the production of ROS and hence the stable expression of HIF-1 as discussed in Chapter 1[4]. Upregulation of HIF-1α induces the expression of distinct angiogenic factors thereby promoting the growth and sustenance of tumor vasculature ultimately promoting cellular growth[5]. Additionally, a recent study has also identified that HIF-1α plays an important role in predicting the radiotherapy response of cancer stem cells (CSC's)[6]. Another study by Lee et al 2018 established that HIF-1 inhibition led to a decrease in glucose catabolism in radiation resistant lung cancer cells[7]. This residual glucose is further employed by the pentose phosphate pathway (PPP) to maintain the NADPH-glutathione buffer that scavenges the reactive oxygen species (ROS) thereby facilitating radiation resistance[8]. Nicotinamide and flavin adenine dinucleotides (NADH and FAD), coenzymes in redox reactions are central to cellular metabolism[9] . Optical Imaging of these biomarkers utilizing the formula FAD/(FAD+NADH), that is, optical redox ratio (ORR) can be used to detect shifts in metabolism, and it corresponded with the mass spectrometry measurements of NAD+/NADH[10].

Perturbations in the cellular metabolism like production of reactive oxygen species (ROS), increase in oxidative phosphorylation (OXPHOS), glucose starvation and exposure to mitochondrial uncouplers drives an increase in redox ratio[7,11,9]. On the contrary, a drop in redox ratio is identified in conditions like exposure to hypoxia, fatty acid synthesis or fatty acid oxidation, macromolecular synthesis etc[12,13].

ORR has been previously utilized to investigate radiosensitive and radioresistant cells and their metabolic response on exposure to radiotherapy[14]. Increase in ORR was observed after inhibition of HIF-1 which was linked to downregulation of pyruvate dehydrogenase kinase (PDK-1) which further obstructs the passage of pyruvate into the mitochondria thereby promoting a surge in the reactive oxygen species (ROS)[15]. These studies have identified the validity of ORR to distinguish metabolic response to therapy in radiosensitive and radioresistant cells. In a recent in vivo study, it was demonstrated that label-free Raman spectroscopy identifies metabolic shifts post radiotherapy in radiosensitive UMSCC22B and radioresistant UMSCC 47 cells[16]. The purpose of this study was to evaluate longitudinal changes in cellular metabolism in response to radiation therapy in a group of radiation-resistant and radiation-sensitive head and neck cancer cell lines. We hypothesize that radiation-resistant cancer cells will demonstrate increased glycolytic metabolism post-radiation that is mediated by HIF-1 to promote cell survival. To evaluate these shifts in cellular metabolism, we employed a panel of head and neck carcinoma cell lines and determined the metabolic changes on exposure to HIF-1α inhibition alone and in combination with radiation as seen in Figure 1.

2. Methods:

2.1 Cell culture, Radiation of cells and suppression of HIF-1α:

The panel of head and neck cell lines used in this study is as follows: UMSCC22B, UMSCC47, 93VU147T and SCC2. UMSCC22B cell line was established from a metastatic lymph node

tumor of a female patient and has been tested negative for Human Papilloma Virus16(HPV16) was obtained from Millipore Sigma. UMSCC47 cells which were also obtained from EMD Millipore were derived from the primary tumor from the lateral tongue of a male patient were found to be HPV-16 positive. 93VU147T cell lines were first isolated from primary tumor from the floor of the mouth of a male patient has been found to be HPV-16 negative. Cells were cultured employing Dulbecco's Modified Eagle's Medium (DMEM) supplemented with 10%(v/v) of Fetal Bovine Serum (FBS), 2 mM L-Glutamine, 1% (v/v) nonessential amino acids, and 1%(v/v) penicillin-streptomycin in a humidified incubator that was set to 5% CO2 and 37℃. UDSCC2 cells were acquired from primary tumor of the hypopharynx of a male patient and found to be HPV-16 positive. These cells were cultured with Dulbecco's Modified Eagle's Medium (DMEM) supplemented with 10%(v/v) of Fetal Bovine Serum (FBS), 2 mM L-Glutamine, 1% (v/v) nonessential amino acids, 1%(v/v) Pyruvate and 1%(v/v) penicillin-streptomycin. Passaging of all the cells was fulfilled at about 80% confluency and were used for all the experiments in the first 10 passages. Irradiation of cells was done to develop radiation resistant cells. Inhibition of HIF-1α was achieved by dosing it with 50 μM (3-(5′-hydroxymethyl-2′-furyl)-1-benzyl indazole (YC-1; Sigma-Aldrich, St. Louis, MO) and equivalent volume of DMSO for 24 hours and 48 hours. Cells exposed to radiation treatment were untreated (0hours) and further radiated to 2Gy of radiation and were imaged at 24 and 48 hours respectively. Biological radiator (X-Rad320, Precision X-ray Inc., North Branford, CT) was used to accomplish radiation. In specimens exposed to combination of YC-1 and radiation treatment, the cells were at first imaged untreated (0hours). After imaging the untreated cells, the specimens were early treated with 50 μM of YC-1 and were further exposed to 2Gy of radiation 5 minutes after the addition of YC-1. These specimens exposed to combination therapy and were imaged at 24 hours and 48 hours post treatment. One independent sample exposed to only YC-1 was imaged untreated (0hours) and 24, 48 hours post treatment.

2.2 Two-photon imaging of cellular autofluorescence:

An optimized cell number was used to plate cells in glass bottom dishes 24-48 hours prior to the experiment. After 48 hours, the dishes were placed in a heated chamber (37˚C) and were imaged at baseline and 24, 48 hours post treatment employing a custom-built, resonant-scanning multiphoton microscope with a MaiTai ultrafast Ti:Sapphire tunable laser source (Spectra Physics, Santa Clara, CA).Laser was excited to 760nm and 850nm for NADH and FAD fluorescence.

Non-descanned GaAsP photomultiplier tubes (H7422-40, Hamamatsu) with 460/40 nm (NADH) or 525/40 nm (FAD) bandpass filters were used to acquire images. 20x water immersion objective (NA = 0.8, working distance = 3.5 mm, diffraction-limited lateral resolution = 0.6 μm) was adopted to acquire images (256 x 256 pixels; 16-bit depth; 130 μm x 130 μm). MATLAB was used for analyzing images. The ratios of FAD/(NADH+FAD) fluorescence were used to generate optical images by computing their pixel wise values. The average values of NADH and FAD intensities were quantified from their corresponding images separately and the ratio of these values were further used to calculate the average redox ratio of each cell plate for the purpose of data representation and statistical analysis. For each cell line, separate plates were imaged for all the treatment conditions and were imaged at 0(untreated), 24 and 48 hours post treatment. Image acquisition was done using three fields of view in each cell plate and 6 random cells were selected within each field of view. Two independent runs of these experiments were performed.

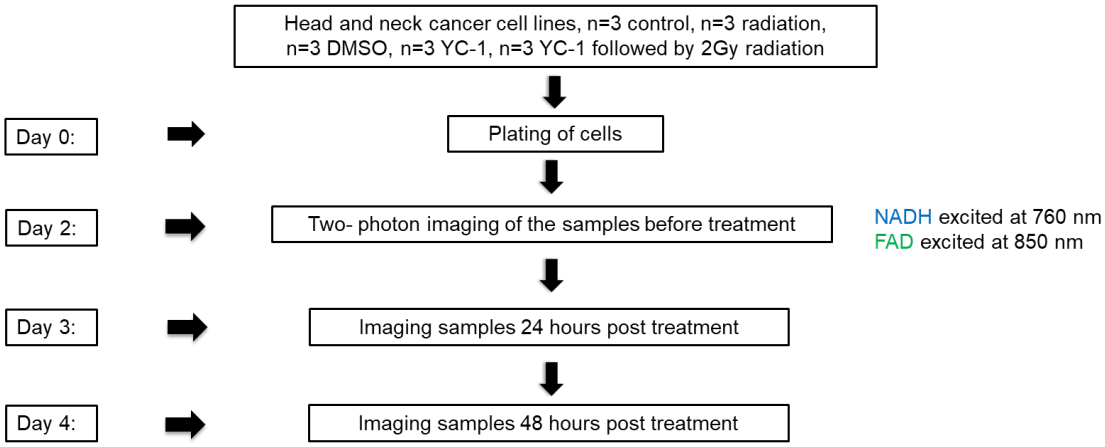

Figure 1. Experimental set up of a panel of head and neck cancer cells on exposure to radiation, HIF-1α inhibitor and a combination treatment of YC-1 followed by radiation together with control.

2.3 Statistical analysis

A nested, two-way analysis of variance (ANOVA) was employed to determine the statistically significant differences in the average redox ratio. Treatment and the time points on exposure to treatment were considered under the fixed effects category while the cell plates and fields of view within each group were considered as random effects. Interactions between all effects were also considered. Post-hoc Tukey HSD tests were used to assess statistical significance between cell groups.

3. Results:

3.1 Radiation-sensitive and HPV16-negative UM-SCC-22B cells are minimally perturbed by YC-1 and radiation therapy

UMSCC22B radiation sensitive cells were exposed to 2Gy radiation, 50μM YC-1 that inhibits the HIF-1α pathway, DMSO, and a combination therapy of YC-1 followed by 2Gy radiation after 5 minutes. Representative images for each treatment condition for UMSCC22B cell line are shown in Figure 2A. We found significant increase in ORR 48 hours ($p< 0.01$) post seeding in UMSCC22B cells. Additionally, we also found a significant increase in ORR 24 hours post

exposure to DMSO($p<0.05$) and 48 hours post exposure to DMSO($p<0.01$). However, we did not see any considerable changes in the redox ratio on exposure to YC-1 and radiation therapy.

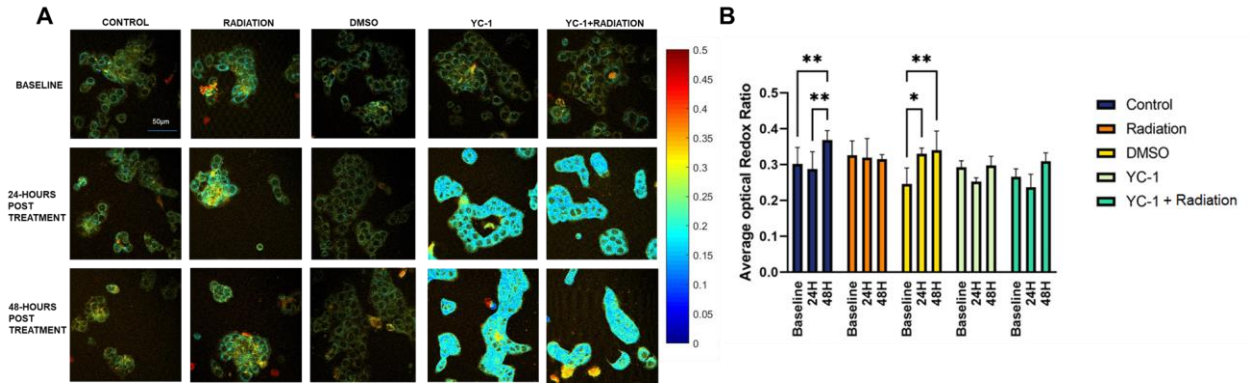

Figure 2. Optical redox ratio shows significant changes in control group and in group exposed to DMSO in radiosensitive UMSCC22B cells. A. Representative redox ratio images of UMSCC22B on exposure to 2Gy radiation, DMSO, YC-1 and YC-1 followed by radiation. We recorded 18 images for each of the time points mentioned above. B. Quantification of mean redox ratios: control, on exposure to 2Gy radiation, DMSO, YC-1 and YC-1 followed by radiation. The seeding density for each cell line was individually optimized before the actual experiments. Experiments were performed in triplicate across 2 independent experiments. Error bars represent standard deviation of the mean, n=2. Asterisks placed above bars indicate statistical significance. * ** and *** denotes statistical significance at $p<0.05$, $p<0.01$ and $p<0.001$ respectively.

3.2 Exposure to radiation causes an increase in the redox ratio of radiation-sensitive and HPV-16 positive UD-SCC-2 cells

Representative images for UDSCC2 radiation sensitive cells on exposure to 2Gy radiation, 50µM YC-1 that inhibits the HIF-1α pathway, DMSO, and a combination therapy of YC-1 followed by 2Gy radiation after 5 minutes along with control are displayed in Figure 3A. We found significant increase in ORR in cells 48 hours post radiation exposure ($p<0.05$) and 48 hours post exposure to DMSO ($p< 0.01$) in UDSCC2 cells.

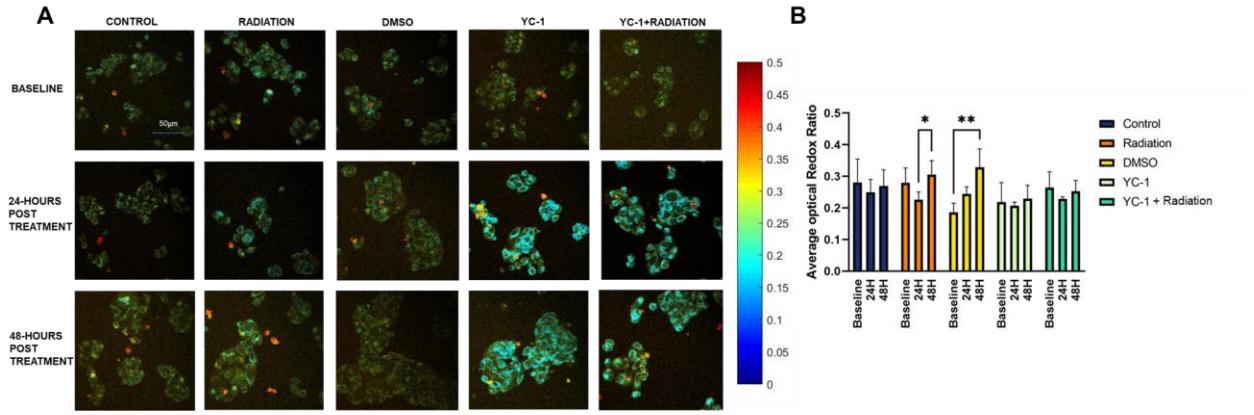

Figure 3. We observe a significant change in the optical redox ratio in control samples and in samples exposed to DMSO in in radiosensitive UDSCC2 cells. A. Representative redox ratio images of UDSCC2 cells on exposure to 2Gy radiation, DMSO, YC-1 and YC-1 followed by radiation along with control. We recorded 18 images for each of the time points mentioned above. B. Quantification of mean redox ratios: control, on exposure to 2Gy radiation, DMSO, YC-1 and YC-1 followed by radiation. The seeding density for each cell line was individually optimized before the actual experiments. Experiments were performed in triplicate across 2 independent experiments. Error bars represent standard deviation of the mean, n=2. Asterisks placed above bars indicate statistical significance. * ** and *** denotes statistical significance at $p<0.05$, $p<0.01$ and $p<0.001$ respectively.

3.3 HPV16-positive and radiation-resistant UMSCC 47 cells are minimally perturbed by exposure to YC-1 and radiation therapy

UMSCC 47 radiation resistant cells were treated to 2Gy radiation, 50μM YC-1 that blocks the HIF-1α pathway, DMSO, and a combination therapy of YC-1 followed by 2Gy radiation after 5 minutes in addition to control samples. Representative images for each treatment condition for UMSCC22B cell line are shown in Figure 4A. We found a significant decrease ($p<0.05$) in the ORR in cells 24 hours post exposure to radiosensitizer YC-1.

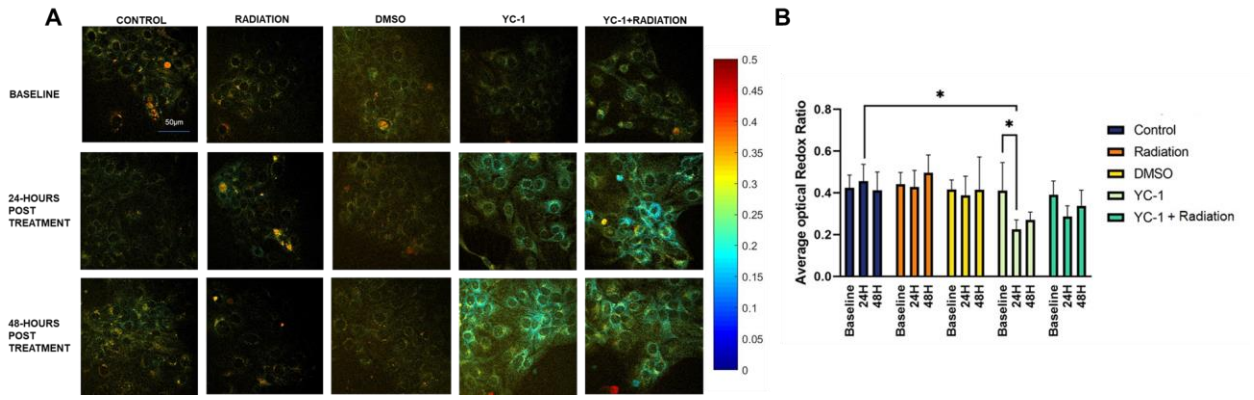

Figure 4. Considerable decrease in optical redox ratio was observed in cells 24 hours post exposure to YC-1 in radiation resistant UMSCC 47 cells. A. Representative redox ratio images of UMSCC 47 cells on exposure to 2Gy radiation, DMSO, YC-1 and YC-1 followed by radiation along with control. We recorded 18 images for each of the time points mentioned above. B. Quantification of mean redox ratios: control, on exposure to 2Gy radiation, DMSO, YC-1 and YC-1 followed by radiation. The seeding density for each cell line was individually optimized before the actual experiments. Experiments were performed in triplicate across 2 independent experiments. Error bars represent standard deviation of the mean, n=2. Asterisks placed above bars indicate statistical significance. * ** and *** denotes statistical significance at $p<0.05$, $p<0.01$ and $p<0.001$ respectively.

3.4 Significant increase in the optical redox ratio is observed on exposure to radiation, YC-1, and combination therapy in 93VU147T cells

Representative images for 93VU147T radiation resistant cells that were exposed to 2Gy radiation, 50µM YC-1 that obstructs the HIF-1α pathway, DMSO, and a combination therapy of YC-1 followed by 2Gy radiation after 5 minutes with control samples are displayed in Figure 5A. Significant increase in ORR ($p<0.05$) is observed 48 hours post exposure to radiation, YC-1 and YC-1 followed by radiation.

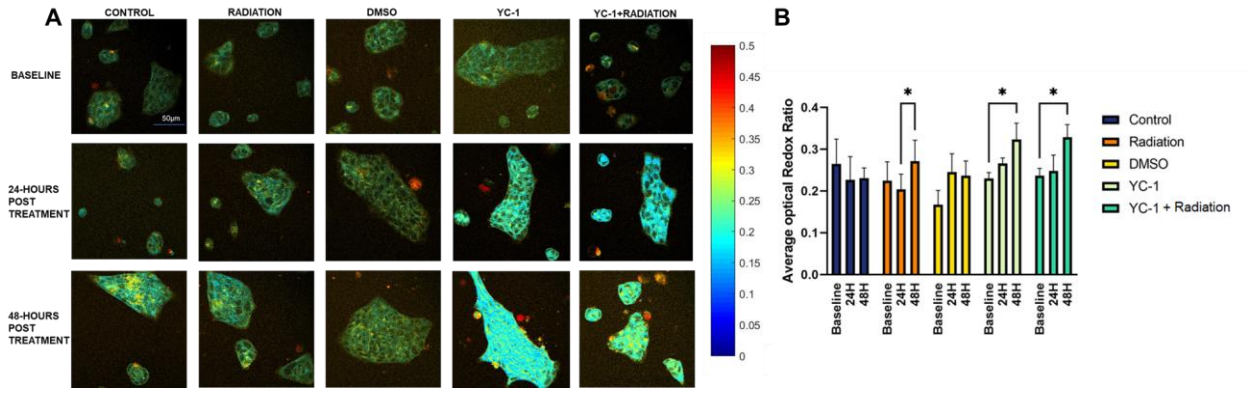

Figure 5. A significant increase in optical redox ratio was observed in cells 48 hours post exposure to radiation, YC-1 and YC-1 in combination with radiation in radioresistant 93VU147T cells. A. Representative redox ratio images of 93VU147T cells on exposure to 2Gy radiation, DMSO, YC-1 and YC-1 followed by radiation along with control. We recorded 18 images for each of the time points mentioned above. B. Quantification of mean redox ratios: control, on exposure to 2Gy radiation, DMSO, YC-1 and YC-1 followed by radiation. The seeding density for each cell line was individually optimized before the actual experiments. Experiments were performed in triplicate across 2 independent experiments. Error bars represent standard deviation of the mean, n=2. Asterisks placed above bars indicate statistical significance. * ** and *** denotes statistical significance at $p<0.05$, $p<0.01$ and $p<0.001$ respectively.

4. Discussion:

There's a large body of knowledge suggesting metabolic reprogramming as a cause of resistance to both radiation as well as chemotherapy[17,18,19]. However, there remains a gap in knowledge regarding the molecular mechanisms that lead to therapeutic resistance. This study has utilized optical imaging to elucidate changes in metabolism on exposure to therapy. Earlier studies from our lab have shown that ORR can be used to predict treatment response in radiosensitive and radioresistant cell lines[20]. In this study, we have found out that UMSCC22B radiosensitive cells show increase in the redox ratio in control and DMSO samples at 48 hours. This upward trend of increase in the redox ratio as compared to basline can be associated with increased proliferation of the cells. No considerable cytotoxic effects were observed in cancer cells with 0.1% DMSO as per the previous studies conducted. This might explain the spike in ORR on exposure to DMSO 24-,48- hours post exposure due to proliferating cancer cells unaffected by DMSO exposure[21].UDSCC2 cells are more radiosensitive than the UMSCC22B.

Low ORR on exposure to radiation can be elucidated for increased radiosensitivity in HPV16 positive cells. A study conducted by Gleber-Netto et al describes the variations in HPV+ tumors as a survival mechanism that can be interpreted by the higher ORR at 48 hours post exposure to radiation[22].Previously, studies have indicated that UMSCC47 cells express higher levels of HIF-1α at normoxia and on exposure to hypoxia[23]. Some of our previous results have elucidated that radio resistant cells exhibit higher redox ratios on HIF-1 inhibition by YC-1[7]. Therefore, more work is needed to investigate this decrease in ORR on 24 hours post exposure to YC-1 Increase in ORR on exposure to radiation in 93VU147T possibly due to G2 moderate arrest and lower number of double stranded break's (DSB's) thereby exhibiting metabolic reprogramming[24]. The increase in ORR is observed in cells on exposure to YC-1 can be possibly due to higher ROS production consequent to HIF-1 inhibition thereby leading to increased proliferation and survival. The combination of YC-1 followed by radiation also saw an increase in ORR 48 post treatment which could be an aftermath of a combination of reduced DSB's and increased ROS production. To further understand the changes in the tumor microenvironment, we should measure glucose uptake using 2-NBDG, HIF-1, PDK-1 expression, and ROS expressions at these timepoints.

In summary, we have identified the metabolic changes in the redox state of the cells 24-,48-hours post treatment employing a non-invasive, nondestructive imaging approach. These time points are extremely crucial as these changes in tumor microenvironment post radiation would lay groundwork for treatment response in clinical settings. Metabolic traits corresponding to the optical redox state were established by employing a combination of radiosensitizer and irradiation that was used to sensitize the radioresistant cells. Our results show that ORR can effectively distinguish radiosensitive effects between distinct radioresistant cells with increasing levels of radiation resistance at 24-, 48- hours post treatment. There is a crucial need for label free methods to pinpoint appropriate treatment choices in patients undergoing radiation or chemotherapy. A preliminary understanding of the time-dependent shifts in cellular metabolism

post radiation and combined chemoradiotherapy have been established with these results. Our future approach would be to investigate these metabolic endpoints in patient- derived organoids, co-culture models and in xenograft animal models.

References:

1. Johnson, D. E. *et al.* Head and neck squamous cell carcinoma. *Nat. Rev. Dis. Prim.* **6**, (2020).

2. Song, S. Radiotherapy for Head and Neck Cancers. *Cancer Consult Expert. Clin. Pract.* **1**, 759–766 (2014).

3. Horsman, M. R., Mortensen, L. S., Petersen, J. B., Busk, M. & Overgaard, J. Imaging hypoxia to improve radiotherapy outcome. *Nat. Rev. Clin. Oncol.* **9**, 674–687 (2012).

4. Beasley, N. J. P. *et al.* Hypoxia-inducible factors HIF-1α and HIF-2α in head and neck cancer: Relationship to tumor biology and treatment outcome in surgically resected patients. *Cancer Res.* **62**, 2493–2497 (2002).

5. Koukourakis, M. I. *et al.* Hypoxia-inducible factor (HIF1A and HIF2A), angiogenesis, and chemoradiotherapy outcome of squamous cell head-and-neck cancer. *Int. J. Radiat. Oncol. Biol. Phys.* **53**, 1192–1202 (2002).

6. Wozny, A. S. *et al.* Differential pattern of HIF-1α expression in HNSCC cancer stem cells after carbon ion or photon irradiation: One molecular explanation of the oxygen effect. *Br. J. Cancer* **116**, 1340–1349 (2017).

7. Lee, D. E. *et al.* A Radiosensitizing Inhibitor of HIF-1 alters the Optical Redox State of Human Lung Cancer Cells in Vitro. *Sci. Rep.* **8**, 1–10 (2018).

8. Mims, J. *et al.* Energy metabolism in a matched model of radiation resistance for head and neck squamous cell cancer. *Radiat. Res.* **183**, 291–304 (2015).

9. Kolenc, O. I. & Quinn, K. P. Evaluating cell metabolism through autofluorescence imaging of NAD(P)H and FAD. *Antioxidants Redox Signal.* **30**, 875–889 (2019).

10. Quinn, K. P. *et al.* Quantitative metabolic imaging using endogenous fluorescence to detect stem cell differentiation. *Sci. Rep.* (2013). doi:10.1038/srep03432

11. Alhallak, K., Rebello, L. & Rajaram, N. Optical imaging of cancer cell metabolism in murine metastatic breast cancer. in *Optics InfoBase Conference Papers* (2016).

12. Hou, J. *et al.* Correlating two-photon excited fluorescence imaging of breast cancer cellular redox state with seahorse flux analysis of normalized cellular oxygen consumption. *J. Biomed. Opt.* (2016). doi:10.1117/1.JBO.21.6.060503

13. Kolenc, O. I. & Quinn, K. P. valuating Cell Metabolism Through Autofluorescence Imaging of NAD(P)H and FAD. doi:10.1089/ars.2017.7451

14. Alhallak, K. *et al.* Optical imaging of radiation-induced metabolic changes in radiation-sensitive and resistant cancer cells Optical imaging of radiation-induced metabolic changes in radiation-sensitive and resistant cancer cells. doi:10.1117/1.JBO.22.6.060502

15. Lee, D. E. *et al.* A Radiosensitizing Inhibitor of HIF-1 alters the Optical Redox State of

Human Lung Cancer Cells In Vitro. *Sci. Rep.* **8**, 8815 (2018).

16. Paidi, S. K. *et al.* Label-free Raman spectroscopy reveals signatures of radiation resistance in the tumor microenvironment. *Cancer Res.* **79**, 2054–2064 (2019).

17. Vidal, R. S., Quarti, J., Rodrigues, M. F., Rumjanek, F. D. & Rumjanek, V. M. Metabolic reprogramming during Multidrug resistance in Leukemias. **8**, 1–9 (2018).

18. Mari, A. *et al.* Genetic determinants for chemo- and radiotherapy resistance in bladder cancer. **6**, 1081–1089 (2017).

19. Levitt, J. M. *et al.* Intrinsic fluorescence and redox changes associated with apoptosis of primary human epithelial cells. *J. Biomed. Opt.* **11**, 064012 (2006).

20. Alhallak, K. *et al.* Optical imaging of radiation-induced metabolic changes in radiation-sensitive and resistant cancer cells. *J. Biomed. Opt.* **22**, 60502 (2017).

21. Trivedi, A. Ben, Kitabatake, N. & Doi, E. Toxicity of Dimethyl Sulfoxide as a Solvent in Bioassay System with HeLa Cells Evaluated yl) -2 , 5-diphenyl-tetrazolium Bromide. **1369**, (2014).

22. Gleber-Netto, F. O. *et al.* Variations in HPV function are associated with survival in squamous cell carcinoma. *JCI Insight* **4**, (2019).

23. Knuth, J. *et al.* Hypoxia-inducible factor-1α activation in HPV-positive head and neck squamous cell carcinoma cell lines. *Oncotarget* **8**, 89681–89691 (2017).

24. Rieckmann, T. *et al.* HNSCC cell lines positive for HPV and p16 possess higher cellular radiosensitivity due to an impaired DSB repair capacity. *Radiother. Oncol.* **107**, 242–246 (2013).

Chapter 4:

Optical metabolic imaging of changes in cell metabolism in a matched model of radiation resistance

1.Introduction:

Oral squamous cell carcinoma (OSCC) comprises of 40% of the total head and neck cancer cases and is considered as one of the most prevalent cancers in humans with 90% of tumors progressing towards malignancy[1]. Surgery followed by radiation or/and chemotherapy is a treatment of choice in OSCC[2,3]. A higher patient mortality is observed in patients with OSCC resulting from radioresistance which can be factually described as resistance of cells, tissues, organs, or entire organisms to the pharmacological aftereffects to radiation therapy[4] .
One of the critical factors contributing towards radiation resistance is tumor hypoxia[5]. Several studies have depicted that hypoxia is a negative prognostic factor in head and neck cancer patients[6,7,8.] Additionally, studies have demonstrated that hypoxia not only negatively affects the patient but also diminishes the effectiveness of radiotherapy, surgery and thereby increases the risk of metastases[9]. The expression of hypoxia in cells is regulated by the transcription factor hypoxia inducible factor- 1α(HIF-1α)[10]. Recently, a study was conducted by Zhang et al evaluating the role of HIF-1α employing a mouse model of sarcoma. This study identified that deletion of HIF-1α results in switches in the cellular response post radiation resulting in higher radiosensitivity, mitochondrial density and mitochondrial biogenesis[11]. Further studies in the Furdui group have detected characteristic metabolic phenotypes with higher reliance on glucose but diverging from the classical Warburg pathway and employing fatty acids to meet the energy demands in radiation resistant cells[12]. Additionally, studies employing proteomics have revealed upregulation and downregulation of several networks like DNA replication and base excision repair, extracellular matrix-receptor interaction, cell cycle, focal adhesion, and regulation of actin cytoskeleton[4].

Metabolic cofactors or coenzymes or electron carriers, nicotinamide adenine dinucleotide (NADH) and flavin adenine dinucleotide (FAD) exhibit endogenous fluorescent biomarkers that play a significant role in cellular metabolism[13]. Quantification of these fluorescent biomarkers employing multiphoton microscopy techniques has been used to detect changes in cellular metabolism. This quantification, known as optical redox ratio (ORR) is defined by the formula: FAD/ (NADH+FAD) and is a validated method that has been adopted to evaluate cellular metabolism[14]. Modifications in cellular metabolism such as production of reactive oxygen species (ROS), increase in oxidative phosphorylation (OXPHOS), glucose starvation and on exposure to mitochondrial uncoupler leads to increase in the redox ratio. Conversely, a decrease in the redox ratio was identified in conditions like exposure to hypoxia, fatty acid oxidation, macromolecular synthesis etc[15,13.] Previously, a study established that ORR could be used to evaluate vital changes in cell metabolism that are characteristic of metastatic ability and invasiveness of the cancer cells[16]. Additionally, another study has identified that radiation resistant cells exhibit a higher expression of HIF-1α and exhibited glycolytic metabolism and propensity towards glycolysis post radiation[17]. Another recent investigation has indicated that ORR could be employed for early detection of radiation resistance in cancer cells. This was established based on early metabolic shifts in cellular metabolism after suppression of HIF-1α[18]. These studies have established the efficacy of label free imaging approach with minimum invasion and photodamage with promising clinical applications to determine metabolic perturbations in cellular metabolism on exposure to treatment. However, there remains a gap in knowledge regarding metabolic changes that are linked with radiation resistance in a panel of oral squamous cell carcinoma lines with a similar genetic background.

The objective of this study was to evaluate the redox variations resulting from differences in cellular metabolism in squamous carcinoma cells with distinct grades of radiation resistance and common genetic makeup on exposure to HIF-1α inhibitor, YC-1. Our underlying hypothesis was that with progressive increase in radiation resistance from the most sensitive to most resistant

cell line, we will observe a shift in baseline cell metabolism towards a more glycolytic phenotype that allows cells to better survive radiation-induced damage. Additionally, we also verified if a combination therapy of YC-1 with radiation exposure would modify the metabolic traits linked with radiation resistance. We assessed the modifications in ORR in wild type and two isogenic clones of radiation-resistant murine squamous carcinoma cell lines on exposure to HIF-1α inhibitor, YC-1, alone and in combination with radiation as seen in Figure 1.

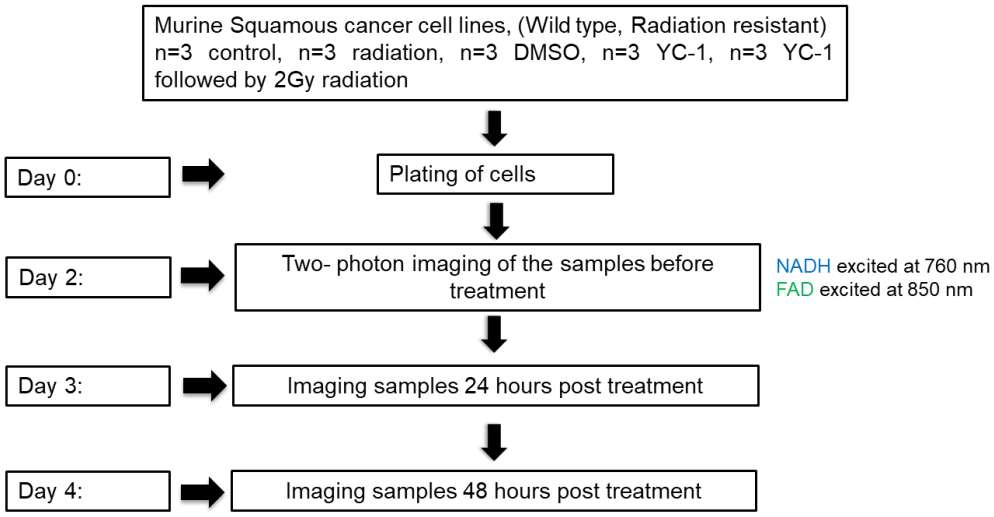

Figure 1. Experimental set up of murine squamous cancer cells on exposure to radiation, HIF-1α inhibitor and a combination treatment of Yc-1 followed by radiation along with the control.

2. Methods

2.1 Cell culture, generation of radiation resistant cells and restriction of HIF-1α pathway

Mouse squamous carcinoma SCC7 cells were obtained as a gift from Dr. Dings's laboratory at UAMS, Little Rock. They were cultured employing Dulbecco's Modified Eagle Medium (DMEM) medium which consists of 10% Fetal Bovine Serum (FBS), 1% penicillin- streptomycin, 1% glutamine, and 1% sodium pyruvate. Irradiation of cells was accomplished employing a biological radiator (X-Rad 320, Precision X-ray Inc., North Branford, CT). Radiation resistant

cells were generated that were resistant to 13 fractions and 26 Gy of radiation (SCC713FX26GY) and 25 fractions and 55 Gy of radiation (SCC726FX55GY) at UAMS. Cells were cultured in T25 flasks and received radiation every 3 days (320 kv 12 mA) after which the media was changed. Cells received 20 fractions of 2 Gy and 5 fractions of 3 Gy totaling 55 Gy. Radiation resistance was confirmed clonogenically at least 2 passages after the final dose of radiation.

To inhibit the HIF-1α pathway, cells were treated with 50 μM (3-(5′-hydroxymethyl-2′-furyl)-1-benzyl indazole (YC-1; Sigma-Aldrich, St. Louis, MO) and equivalent volume of DMSO was used as a control for 0,24 and 48 hours. Cells that were exposed to radiation were untreated (0 hours) and imaged and then further exposed to 2Gy radiation and were imaged at 24 and 48 hours. A combinatorial treatment wherein the cells were first treated with 50 μM YC-1 and after 5 minutes were treated with 2Gy radiation 24-,48- hours post treatment.

2.2 Two photon imaging of NADH and FAD autofluorescence:

A pre-determined cell number were seeded 24 hours prior to experiment. After 24 hours, cells were imaged untreated (0 hours) and were further imaged post treatment at 24-,48 hours respectively. Imaging was accomplished employing a MaiTai Ti:Sapphire laser source (Spectra-Physics, Santa Clara CA) by measuring the endogenous fluorescence of NADH wherein laser was tuned to 760nm for NADH excitation while FAD fluorescence was measured by tuning the laser to 850nm. A resonant-galvo scanner and GaAsP photomultipler tubes (H7422-40, Hamamatsu) with bandpass filters at 440/60 nm (NADH) and 525/45 nm (FAD) were used to capture images. Pixel wise calculation of FAD/(NADH+FAD) ratio were used to produce images.

2.3 Statistical Analysis:

Statistically significant differences in the average redox ratio were evaluated via a nested, two-way analysis of variance (ANOVA). Treatment and the time points on exposure to treatment

were considered fixed effects while the cell plates and fields of view within each group were considered random effects. Interactions between all effects were also considered. Post-hoc Tukey HSD tests were used to evaluate statistical significance between specific cell groups.

3. Results:

3.1 A decrease in redox ratio is exhibited in SCC7 wild type cells 48 hours post initial plating in comparison to baseline values.

SCC7 wild type cells were plated and later imaged untreated. Post untreated imaging, cells were treated with 2Gy radiation, 50µM YC-1, DMSO, combination therapy of YC-1 followed by radiation along with control sample. Representative images at each time point from each cell line are shown in Figure 2. We observed a lower redox ratio in untreated cells 48 hours post plating($p<0.05$). Decrease in the redox ratio 48 hours post radiation exposure was also detected in wild type SCC7 cells($p<0.05$). Additionally, SCC7 cells also demonstrated a lower ORR 48 hours post exposure to Dimethyl sulfoxide (DMSO) ($p<0.01$). Finally, a significant decline in redox ratio was also observed 24-, 48- hours post exposure to YC-1 and combination therapy of YC-1 and radiation, ($p<0.01$ and $p<0.001$).

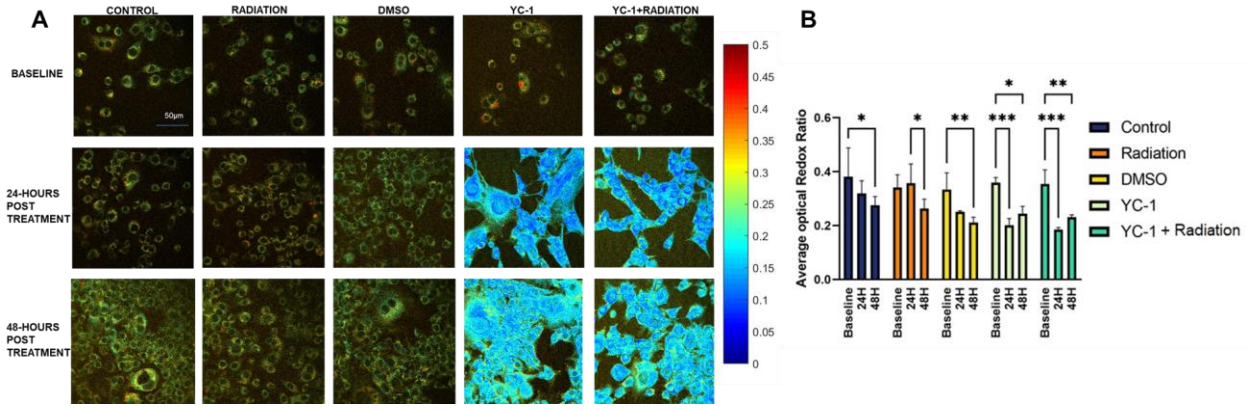

Figure 2. Exposure to diverse therapies causes significant changes in the optical redox ratio in SCC7 wild type cells in all the conditions. We recorded 18 images for each of the time points

mentioned above. A. Representative redox ratio images of SCC7 wild type cells on exposure to treatments along with the control. B. Quantification of mean redox ratios for SCC7 wild type cells at baseline(untreated), 24-,48-hours post treatment. The seeding density for SCC7 wild type cells cell was optimized before the actual experiments. Experiments were performed in triplicate across 2 independent experiments. Error bars represent standard deviation of the mean, n=2. Asterisks placed above bars indicate statistical significance. * ** and *** denotes statistical significance at p<0.05, p<0.01 and p<0.001 respectively.

3.2 HIF-1α inhibition in SCC713FX26GY radiation resistant cells demonstrated a significant decrease in the redox ratio 24 hours post exposure to YC-1 and combination treatment

SCC7 cells that are resistant to 13 fractions and 26Gy of radiation were treated with 2Gy radiation, 50µm YC-1 and a combination treatment of YC-1 followed by radiation after 5 minutes. We observed that these cells exhibited a considerable decrease in the redox ratio 24 hours post exposure to YC-1 (p<0.01) (Figure 3) and combination treatment of YC-1 with radiation(p<0.01) No significant differences were observed between any other treatment groups.

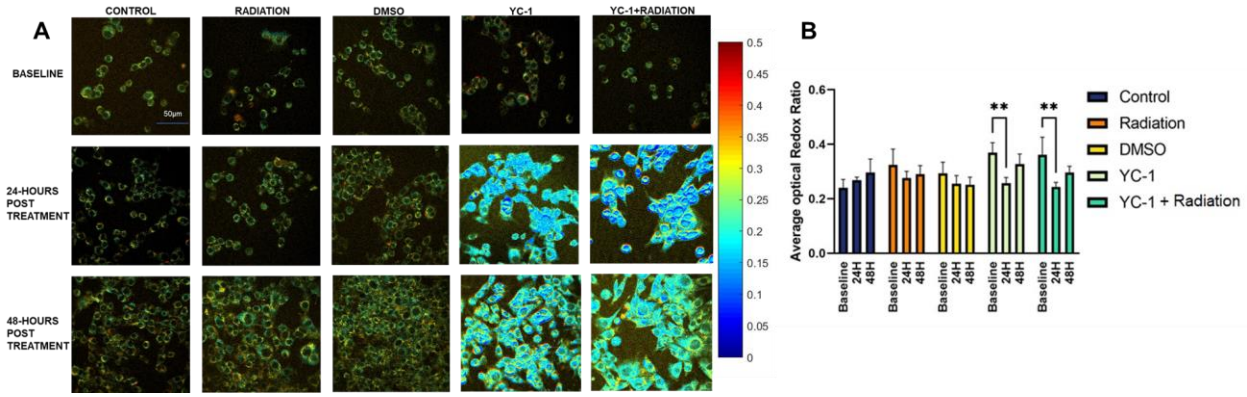

Figure 3. SCC713FX26GY radiation resistant cells exhibited a considerable decrease in the redox ratio 24 hours post exposure to YC-1 and combination treatment. A. Representative redox ratio images of SCC713FX26GY radiation resistant cells on exposure to treatments along with the control. We recorded 18 images for each of the time points mentioned above.
B. Quantification of mean redox ratios for SCC713FX26GY radiation resistant cells at baseline(untreated), 24-,48-hours post treatment. The seeding density for SCC713FX26GY radiation resistant cells were optimized before the actual experiments. Experiments were performed in triplicate across 2 independent experiments. Error bars represent standard deviation of the mean, n=2. Asterisks placed above bars indicate statistical significance. * ** and *** denotes statistical significance at p<0.05, p<0.01 and p<0.001 respectively.

3.3 No significant changes were observed in the redox ratio on exposure to any treatment in SCC726FX55GY radiation resistant cell lines

SCC7 that are resistant to 26 fractions and 55Gy of radiation didn't have any substantial effect to any treatment conditions at baseline(untreated), 24 and 48 hours post treatment (Figure 4).

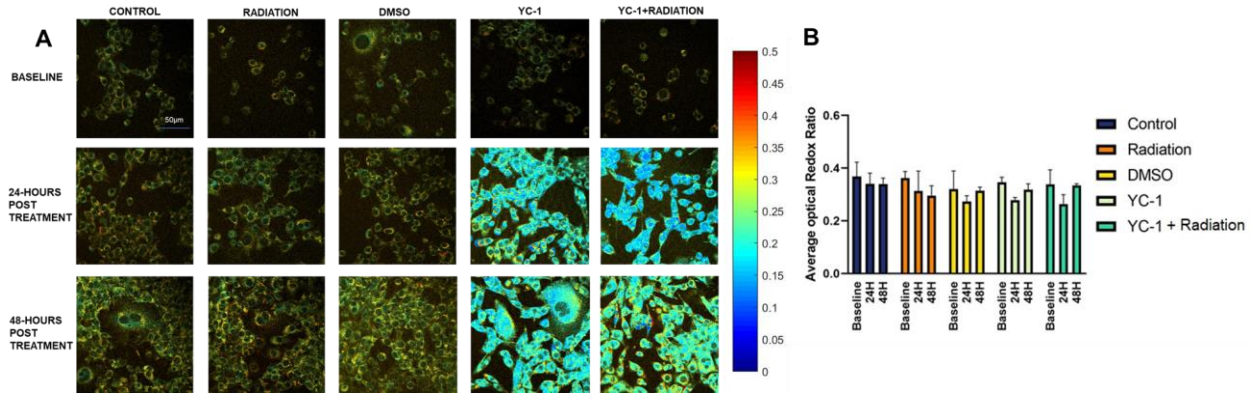

Figure 4. SCC726FX55GY radiation resistant cell lines did not exhibit a considerable decrease in the redox ratio on exposure to any treatment. A. Representative redox ratio images of SCC726FX55GY radiation resistant cells on exposure to treatments along with the control. We recorded 18 images for each of the time points mentioned above. B. Quantification of mean redox ratios for SCC726FX55GY radiation resistant cells at baseline(untreated), 24-,48-hours post treatment. The seeding density for SCC726FX55GY cells were optimized before the actual experiments. Experiments were performed in triplicate across 2 independent experiments. Error bars represent standard deviation of the mean, n=2.

3.4 We observed significant differences in the redox ratio on exposure to YC-1 and YC-1 with radiation in murine squamous cancer cells.

We calculated the difference in the redox ratio between 24-,48- hours post treatment and corresponding untreated groups for each cell line. We found considerable differences in the ORR on exposure to YC-1 and in combination with YC-1 with radiation (Figure 5). This change in ORR could be possibly related to the radioresistance of the cells.

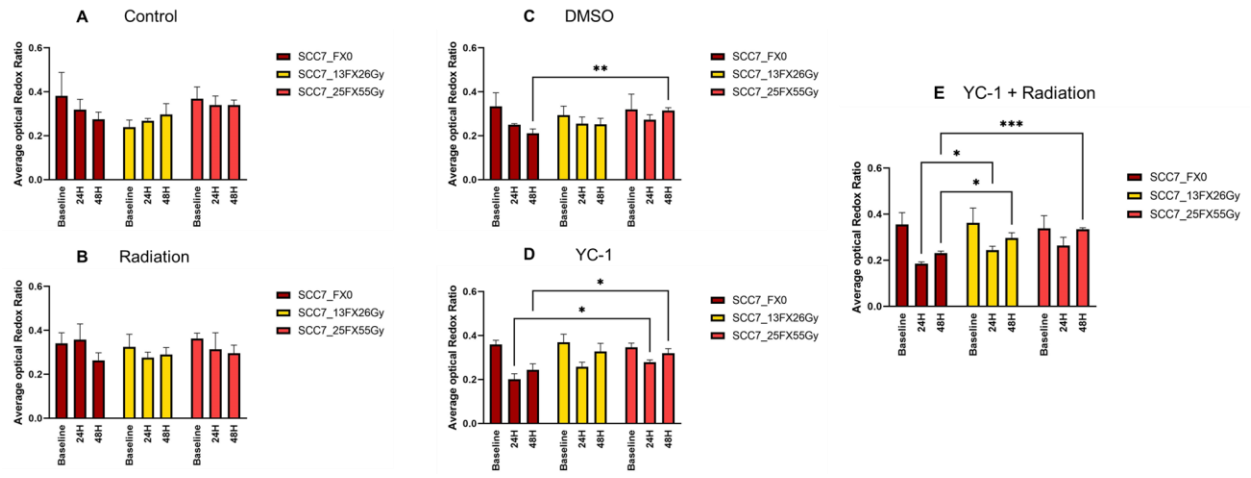

Figure 5. Significant differences in optical redox ratio were observed 24-,48- hours post exposure to YC-1 and in combination with radiation in radioresistant cells. Bar plots represent the difference in the mean values of redox ratio on exposure to A. Untreated/ Control B. Radiation C. DMSO D. YC-1 and E. YC-1+Radiation.

4. Discussion:

Treatment failure due to resistance to radiotherapy is the leading cause of death in patients with OSCC[19,20] Although many studies have pointed out metabolic adaptations in cells as a cause of treatment failure, there remains a lack of non-destructive method to quantify these changes. In this study, we have elucidated the metabolic reprogramming linked with radiation resistance in cell lines with a universal genetic background employing optical imaging. Optical imaging employing ORR has indicated effectiveness in identifying variations in different metabolic pathways in distinct cellular subtypes emulating changes in glycolysis and corresponding oxidative phosphorylation[20,21]. In SCC7 wild type cells we observed lower redox ratio 48 hours post seeding. Previously studies have indicated decrease in the redox ratio reflecting the changes in cell metabolism like macromolecular synthesis, exposure to hypoxia, fatty acid oxidation, cell death etc[13,15,22,23]. 0.1% DMSO which has been used in our study doesn't contribute to any considerable cytotoxic effects in cancer cells consequently leading to proliferation of cancer cells[24].

Decrease in the ORR 24 hours post YC-1 exposure in SCC713FX26GY cells may be due to inhibition of pyruvate dehydrogenase kinase 1 (PDK1) whose expression is controlled by HIF-1 leading to reduced production of Acetyl CoA thereby suspending the TCA cycle[25,18]. Studies have demonstrated that inhibition of HIF-1 induces decreased rate of glucose uptake and lactate production in vitro which could have manifested into decreased cellular metabolism and lower redox ratio[26]. This decline in the redox ratio can also be explained by an in vivo study wherein HIF-1 inhibition followed by radiation increased the tumor hypoxia and thereby curbed the effect of radiation[27].

The most radioresistant cell line SCC726FX55GY didn't exhibit any significant changes in the redox ratio on exposure to any treatment. Lately a study by Jonsson et al emphasized that radioresistant cells modified their cellular metabolism to manipulate the redox status of the cells, regulate DNA repair and transformed DNA methylation post radiation[28]. A study conducted by Mims et al delving into tumor cell metabolism in radiation resistant cells have highlighted key metabolic features as follows: 1. Higher glucose uptake along with decline in fatty acid uptake; 2. Diverging from the Warburg effect and switching towards the pentose phosphate pathway; 3. Higher reliance on glucose metabolism than glutamine metabolism assisting growth of the cells 4. Diminished mitochondrial oxidative phosphorylation; 5. Higher expression of fatty acid synthase resulting into boost of fatty acid biosynthesis; and 6. Exploiting fatty acids to comply with the energy requirements needed for cell proliferation[29]. Another study on head and neck cancer has identified 4 key transcription factors that are linked to radioresistance. These key factors are as follows: focal adhesion, PI3K-Akt signaling, HIF-1 signaling, and pluripotency of stem cells[30]. Lately a study by Ishigami et al has identified 25 genetic signatures that are highly expressed in radioresistant cells as compared to radiosensitive cells in OSCC[31].

To better understand the changes in redox ratio, we need to execute proteomic studies that can give us a definite scientific interpretation of the changes in metabolism in relation to protein

upregulation or downregulation. Additionally, our future studies would focus on conducting cell viability studies in these cell lines utilizing these timepoints.

References:

1. Li, Q. *et al.* Mouse Tumor-Bearing Models as Preclinical Study Platforms for Oral Squamous Cell Carcinoma. *Front. Oncol.* **10**, 1–21 (2020).

2. Fan, H. *et al.* Aberrant Kank1 expression regulates YAP to promote apoptosis and inhibit proliferation in OSCC. *J. Cell. Physiol.* **235**, 1850–1865 (2020).

3. Skinner, H. D. *et al.* Integrative analysis identifies a novel AXL-PI3 kinase-PD-L1 signaling axis associated with radiation resistance in head and neck cancer. *Clin. Cancer Res.* **23**, 2713–2722 (2017).

4. Bansal, N. *et al.* Broad phenotypic changes associated with gain of radiation resistance in head and neck squamous cell cancer. *Antioxidants Redox Signal.* **21**, 221–236 (2014).

5. Janssen, H. L., Haustermans, K. M., Balm, A. J. & Begg, A. C. Hypoxia in head and neck cancer: How much, how important? *Head and Neck* (2005). doi:10.1002/hed.20223

6. Gong, L. *et al.* Prognostic Value of HIFs Expression in Head and Neck Cancer: A Systematic Review. *PLoS One* **8**, (2013).

7. Van Der Heijden, M. *et al.* Acute hypoxia profile is a stronger prognostic factor than chronic hypoxia in advanced stage head and neck cancer patients. *Cancers (Basel).* **11**, (2019).

8. Brizel, D. M., Sibley, G. S., Prosnitz, L. R., Scher, R. L. & Dewhirst, M. W. Tumor hypoxia adversely affects the prognosis of carcinoma of the head and neck. *Int. J. Radiat. Oncol. Biol. Phys.* **38**, 285–289 (1997).

9. Walsh, J. C. *et al.* The clinical importance of assessing tumor hypoxia: Relationship of tumor hypoxia to prognosis and therapeutic opportunities. *Antioxidants Redox Signal.* **21**, 1516–1554 (2014).

10. Goda, N. & Kanai, M. Hypoxia-inducible factors and their roles in energy metabolism. *Int. J. Hematol.* **95**, 457–463 (2012).

11. Zhang, M. *et al.* HHS Public Access. **183**, 594–609 (2016).

12. Mims, J. *et al.* Energy metabolism in a matched model of radiation resistance for head and neck squamous cell cancer. *Radiat. Res.* **183**, 291–304 (2015).

13. Georgakoudi, I. & Quinn, K. P. Optical Imaging Using Endogenous Contrast to Assess Metabolic State. *Annu. Rev. Biomed. Eng.* (2012). doi:10.1146/annurev-bioeng-071811-150108

14. Quinn, K. P. *et al.* Characterization of metabolic changes associated with the functional development of 3D engineered tissues by non-invasive, dynamic measurement of individual cell redox ratios. *Biomaterials* (2012). doi:10.1016/j.biomaterials.2012.04.024

15. Kolenc, O. I. & Quinn, K. P. Evaluating cell metabolism through autofluorescence imaging

of NAD(P)H and FAD. *Antioxidants Redox Signal.* **30**, 875–889 (2019).

16. Alhallak, K. *et al.* Optical redox ratio identifies metastatic potential-dependent changes in breast cancer cell metabolism. *Clin. Oncol* **34**, 2303–2311 (2016).

17. Alhallak, K. *et al.* Optical imaging of radiation-induced metabolic changes in radiation-sensitive and resistant cancer cells. *J. Biomed. Opt.* **22**, 60502 (2017).

18. Lee, D. E. *et al.* A Radiosensitizing Inhibitor of HIF-1 alters the Optical Redox State of Human Lung Cancer Cells in Vitro. *Sci. Rep.* **8**, 1–10 (2018).

19. Almangush, A., Leivo, I. & Mäkitie, A. A. Biomarkers for Immunotherapy of Oral Squamous Cell Carcinoma: Current Status and Challenges. *Front. Oncol.* **11**, 1–5 (2021).

20. Sharma, K. *et al.* Prognostic factors, failure patterns and survival analysis in patients with resectable oral squamous cell carcinoma of the tongue. *Radiat. Oncol. J.* **37**, 73–81 (2019).

21. Alhallak, K. *et al.* Optical imaging of radiation-induced metabolic changes in radiation-sensitive and resistant cancer cells Optical imaging of radiation-induced metabolic changes in radiation-sensitive and resistant cancer cells. doi:10.1117/1.JBO.22.6.060502

22. Alam, S. R. *et al.* Investigation of Mitochondrial Metabolic Response to Doxorubicin in Prostate Cancer Cells: An NADH, FAD and Tryptophan FLIM Assay. *Sci. Rep.* **7**, 1–10 (2017).

23. Levitt, J. M. *et al.* Intrinsic fluorescence and redox changes associated with apoptosis of primary human epithelial cells. *J. Biomed. Opt.* **11**, 064012 (2006).

24. Trivedi, A. Ben, Kitabatake, N. & Doi, E. Toxicity of Dimethyl Sulfoxide as a Solvent in Bioassay System with HeLa Cells Evaluated yl) -2 , 5-diphenyl-tetrazolium Bromide. **1369**, (2014).

25. Park, J. *et al.* CCL28-induced RARβ expression inhibits oral squamous cell carcinoma bone invasion. *J. Clin. Invest.* **129**, 5381–5399 (2019).

26. Harada, H. *et al.* Treatment regimen determines whether an HIF-1 inhibitor enhances or inhibits the effect of radiation therapy. *Br. J. Cancer* **100**, 747–757 (2009).

27. Meijer, T. W. H., Kaanders, J. H. A. M., Span, P. N. & Bussink, J. Targeting hypoxia, HIF-1, and tumor glucose metabolism to improve radiotherapy efficacy. *Clin. Cancer Res.* **18**, 5585–5594 (2012).

28. Jonsson, E. L. *et al.* Exploring radiation response in two head and neck squamous carcinoma cell lines through metabolic profiling. *Front. Oncol.* **9**, 1–16 (2019).

29. Cross, Sarah J. Linker, Kay E. Leslie, F. M. 乳鼠心肌提取 HHS Public Access. *Physiol. Behav.* **176**, 100–106 (2016).

30. You, G. R. *et al.* Prognostic signature associated with radioresistance in head and neck cancer via transcriptomic and bioinformatic analyses. *BMC Cancer* **19**, 1–11 (2019).

31. Ishigami, T. *et al.* Genes and molecular pathways related to radioresistance of oral squamous cell carcinoma cells. *Int. J. Cancer* **120**, 2262–2270 (2007).

Chapter 5:

Discussion and Future Steps

One of the leading causes of deaths in United States (US) is cancer. Most of these deaths are a result of treatment resistance that maybe inherent (intrinsic) prior to treatment or a consequence of therapy (acquired) leading to metastatic recurrence[1]. One of the critical factors that promotes treatment resistance is tumor hypoxia or lack of oxygen and its transcription factor hypoxia-inducible factor (HIF-1)[2,3]. Clinical studies in patients have demonstrated that higher expression of HIF-1 is associated with higher metastatic risk and lower survival[4]. Although studies have pointed that tumor hypoxia is responsible for treatment resistance and has been directly associated to metastases, there remains a gap in knowledge regarding understanding the role of metabolic changes in tumor cells that might contribute to treatment resistance and tumor metastases.

Nicotinamide Adenine Dinucleotide (NADH) and Flavin Adenine Dinucleotide (FAD) are metabolic coenzymes that play a critical role in cellular metabolism[5]. Optical imaging of these biomarkers utilizing two-photon excited fluorescence (TPEF) has provided a quantitative assessment of the cell metabolism. Previously, studies have proved that optical redox ratio (ORR), that is ratio of FAD/(NADH+FAD) has been used to track changes in cell metabolism *in vitro and in vivo*[6].

We started our study with three objectives: to identify the metabolic effects of chronic and intermittent hypoxia in murine breast cancer cells and its association with metastatic potential, to evaluate the effects of radiation therapy on cellular metabolism in a panel of radiation-sensitive and resistant human head and neck cancer cells and to identify the changes in cellular metabolism associated with acquisition of treatment resistance.

To fulfill our first objective, we employed a 2D isogenic murine breast cancer model to study the effects of hypoxic exposures on tumor cell metabolism. Chronic hypoxia, that is, continuous

hypoxic exposure for a period and intermittent hypoxia, that is, hypoxia followed by normoxia at regular time intervals. Chronic hypoxic exposure revealed a significant difference in cellular metabolism in poorly metastatic 168FARN cells owing to glycolysis. Highly invasive 4T1 cells exhibited a higher glycolytic output on post chronic hypoxia. Previously,4T1 cells have exhibited propensity towards both oxidative phosphorylation (OXPHOS) and glycolysis. This shift from OXPHOS to glycolysis assists the need for higher ATP thereby supporting the peculiar traits of uncontrolled growth and proliferation which are one of the key hallmarks of cancer. No considerable changes in cellular metabolism were observed in isogenic murine cancer cells post intermittent hypoxia. However, we did observe an increase in the redox ratio post intermittent hypoxia as compared to normoxic counterparts. Reactive oxygen species (ROS) is associated with an increase in the optical redox ratio as per previous studies conducted in our lab. Since intermittent hypoxia has demonstrated an increase in the redox ratio, we are currently investigating if our results are owing to an increase in ROS. Another aspect of investigation would be to test the HIF-1α expression at normoxia, 0,60-,120 minutes post chronic and intermittent hypoxia. Testing the levels of HIF-1α would provide a supplementary data in addition to the metabolic imaging that could be used to link to our results. If HIF-1α levels are detected, CAIX levels should be tested as well. CAIX is involved in lowering the pH of the tumor microenvironment making it more acidic. Detection of CAIX could possibly explain the glycolytic output we see in our cells on exposure to hypoxia.

To address our second objective, we utilized a panel of radiation-sensitive and resistant human head and neck cancer cells. The rationale for this study was to determine the shifts in cellular metabolism in response to radiation therapy in a group of radiation-resistant and radiation-sensitive cell lines. Higher redox ratio was observed in more radiation resistant 93VU147T as compared to UMSCC47 cells on exposure to radiation, radiosensitizer YC-1, and combination therapy of YC-1 followed by radiation. This result was concurrent with one of the previous publications in the lab. Determining the HIF-1α, PDK-1 expressions in these cell lines would

help us better understand the A higher redox ratio was observed in UDSCC2 cells as compared to UMSCC22B on exposure to radiation. UDSCC2 cells are HPV positive and variations in HPV positive tumors are associated with survival due to deregulated pathways observed in the cellular metabolism.

To address our third objective, we have evaluated the effects of radiation therapy in a panel of isogenic murine squamous cancer cell lines that have been engineered to have increasing levels of radiation resistance. We observed a considerable difference in the cellular metabolism in all treatment conditions in wild type murine squamous cancer cells. Radiosensitivity to YC-1 and a combination of YC-1 with radiation was observed in a moderately radiation resistant cells. Furthermore, no differences in the cellular metabolism in the most radiation resistant cells on exposure to any therapy. Proteomic analysis of head and neck cancer cells and isogenic murine squamous cancer cells 24-,48- hours post treatment will be able to shed light on protein expression post therapy and its impact on radiation resistance.

Our research was designed to identify the effects of microenvironmental stresses on tumor cell metabolism employing nondestructive and label-free optical imaging. Our findings suggest that the chronic exposure to hypoxia has exhibited considerable difference in cellular metabolism in only 168FARN cells that are poorly metastatic. Conversely, we do observe an increase in the redox ratio post intermittent hypoxia, but it didn't exhibit a significant difference in redox ratio. We are currently probing if this increase is a consequence of increase in reactive oxygen species (ROS).

We also identified that redox ratio could differentiate between radiosensitive effects in cellular metabolism in different radioresistant cells with increasing levels of radiation resistance at 24-, 48- hours post treatment. Moreover, we also demonstrated that redox ratio could distinguish between cellular metabolism in radiosensitive cells of variable radiosensitivities. Furthermore, we investigated the changes in cellular metabolism associated with acquisition of treatment resistance by exposing a panel of isogenic cell lines that have been devised to have increasing

levels of radiation resistance to radiation therapy. Our results show that a difference in redox ratio as an output of cellular metabolism is observed in wild type cells on exposure to 24-,48-hours post therapy. Additionally, we identified an increase in redox ratio 24 hours post YC-1 and combination therapy depicting an increase in radiosensitivity in a radioresistant cells. Conversely, no effect in redox ratio was observed in highly radioresistant cells. These findings further our knowledge of metabolic shifts within cancer cells that may contribute to treatment resistance and tumor metastases.

Our future steps will focus on combining these results with transcriptomics to determine which pathways are activated or deactivated in resistant and non-resistant cells with similar timepoints. This would provide a deeper understanding of shifts in the cellular metabolic activity that are controlled by gene expressions. Although majority of the studies have employed 2D invitro cell models to investigate tumor cell metabolism, it would be advantageous to study the interactions of cancer cells with its neighboring cells in a co-culture setting or organoids derived from patient's tumor samples that mimic the tumor microenvironment after exposure to hypoxia or other treatments. For a co-culture study, cells would be imaged in a 2D setting at baseline and on exposure to hypoxia. A training model would be used to train a machine learning algorithm and would be used to correlate it with the output. Once the algorithm is trained it would be used to identify cells in the co-culture settings. After recognition of these cells employing machine learning, experimental conditions would be further tested. In case of organoids, heterogenous population can be differentiated using machine learning and a secondary endpoint employing flow cytometry would be employed to distinguish between different cell populations and their gene expression. Mathematical modeling simulating switches in cellular metabolism in radiation resistance and varying hypoxic durations is another method that could provide further insights into understanding the long-term effects of hypoxia and radiation on cancer cells. Furthermore, an in vivo study employing xenografts would highlight the differences in tumor cell metabolism in

response to therapy as compared to studies accomplished in an in vitro (2D, co-culture and 3D) settings.

References:

1. Wang, X., Zhang, H. & Chen, X. Drug resistance and combating drug resistance in cancer. (2019). doi:10.20517/cdr.2019.10

2. Chen, S. & Sang, N. HHS Public Access. 117, 267–278 (2016).

3. Muz, B. et al. The role of hypoxia in cancer progression, angiogenesis, metastasis, and resistance to therapy. doi:10.2147/HP. S93413

4. Santos, M. dos et al. HIF1-Alpha Expression Predicts Survival of Patients with Squamous Cell Carcinoma of the Oral Cavity. PLoS One 7, (2012).

5. Georgakoudi, I. & Quinn, K. P. Optical imaging using endogenous contrast to assess metabolic state. Annu. Rev. Biomed. Eng. 14, 351–367 (2012).

6. Kolenc, O. I. & Quinn, K. P. Evaluating cell metabolism through autofluorescence imaging of NAD(P)H and FAD. Antioxidants Redox Signal. 30, 875–889 (2019).

7. Lee, D. E. et al. A Radiosensitizing Inhibitor of HIF-1 alters the Optical Redox State of Human Lung Cancer Cells In Vitro. Sci. Rep. 8, 8815 (2018).